Thesis for the degree of Doctor of Philosophy
in the Natural Sciences

Light and X-ray scattering investigations of microtubules subjected to oscillating electric fields

Per Börjesson

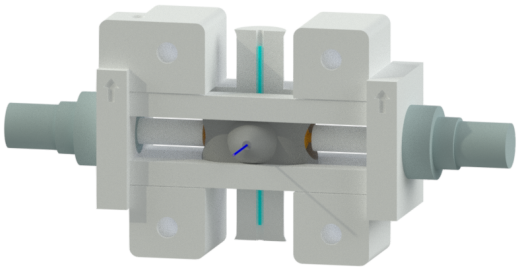

UNIVERSITY OF GOTHENBURG

Department of Chemistry and Molecular Biology
Gothenburg, 2022

Thesis for the degree of Doctor of Philosophy
in the Natural Sciences

Light and X-ray scattering investigations of microtubules subjected to oscillating electric fields

Per Börjesson

Cover: 3D rendering of device used to deliver AC fields to microtubules (**paper 2**).

ISBN 978-91-8069-087-4 (Print)
ISBN 978-91-8069-088-1 (PDF)
Available online at http://hdl.handle.net/2077/74094

Department of Chemistry and Molecular Biology
Division of Biochemistry and Structural Biology
University of Gothenburg
SE-405 30, Göteborg, Sweden
Printed by Stema Specialtryck AB
Borås, Sweden, 2022

Abstract

In our daily lives we are exposed to a wide variety of oscillating electrical fields of different frequencies. These fields stem from devices and technologies that include mobile phones, wifi, bluetooth, navigation radar, automobile radar, communications satellites, and global positioning systems. Public concern regarding possible health effects brought on by exposure to said fields has risen, and investigations into any such effects have given rise to controversy.

Microtubules are tubular protein assemblies built up by smaller dimers, α- and β-tubulin. They are a major component of the cytoskeleton and have many functions such as maintaining the cell's shape, organizing molecules in the cytoplasm, aiding in internal transport of intracellular structures, and separating the chromosomes during cell division. Due to the essential role microtubules play in cell division and function and the fact that microtubules have a high dipole moment, they make an interesting target when investigating the biological effects of oscillating electric fields.

In this thesis we have investigated the effect of oscillating electric fields at different frequencies ranging from 100 kHz to 30 GHz on microtubule polymerization and structure using light and X-ray scattering. We have also attempted to obtain the structure of microtubules in a liquid solution by use of an X-ray laser.

We found no, or little, effect on microtubule structure or polymerization kinetics as a result of the electric field frequencies we tried, with a possible exception of faster polymerization in the 150 kHz range. Our attempt at the reconstruction of the microtubule structure yielded a large diffraction dataset that will require further analysis.

Sammanfattning

I vårt dagliga liv blir vi utsatta för oscillerande elektriska fält av olika frekvenser. Dessa fält inkluderar mobiltelefoner, wifi, bluetooth, radar för navigering, radar från bilar, kommunikationssatelliter, samt GPS. Oro från allmänheten har växt rörande möjlig hälsopåverkan från elektriska fält av dessa typer och undersökningar som gjorts kring möjlig hälsopåverkan har gett upphov till kontrovers.

Mikrotubuler är tubformade proteinsammansättningar som är uppbyggda av mindre dimerer bestående av α- och β-tubulin. De är en viktig komponent i cytoskelettet och fyller en mängd funktioner såsom bibehållning av cellstruktur, organisation av molekyler i cytoplasman, bidrag vid förflyttning av intracellulära strukturer, samt separation av kromosomer vid celldelning. Tack vare mikrotubulernas essentiella roll vid både celldelning och i cellfunktion, samt mikrotubulernas höga dipolmoment, utgör de ett intressant mål för studier av biologiska effekter som resultat av oscillerande elektriska fält.

I denna avhandling har vi undersökt effekterna av oscillerande elektriska fält med olika frekvenser mellan 100 kHz och 30 GHz på mikrotubulernas struktur och polymerisering med hjälp av röntgen samt ljusspridning. Vi har också försökt återskapa mikrotubulens struktur när de befinner sig i en flytande lösning, detta med hjälp av röntgenlaser.

Vi hittade ingen, eller väldigt liten, effekt på mikrotubulernas struktur eller polymerisering som direkt följd av oscillerande elektriska fält, med ett möjligt undantag för förändrad polymerisering i 150 kHz området. Vårt försök att återskapa mikrotubulstrukturen gav en hög mängd diffraktionsdata som kommer kräva vidare analys.

Acknowledgements

First of all my supervisor, **Richard**, thank you for giving me the opportunity to do this PhD. I have appreciated the knowledge you have imparted on me, not only when it comes to science, but also politics, New Zealand colloquialism, and cricket (although knowing myself the latter will fade from my mind quite quickly). Your enthusiasm and kindness has helped me during some of the steeper slopes in my PhD. I hope you will have a calmer schedule in the coming year.

My co-supervisor, **Thomas**, you have been a great help and a calming presence throughout my project. Armed with your big thermos of coffee (which probably helped), you have always taken time for my questions and inquiries. **Douglas**, thank you for sharing an office with me at Chalmers, I hope I was not too intrusive! Your insights were deeply helpful in the development of my electric field device. Good luck with your work at RISE!

Johanna, my extra co-supervisor, although we spent little time together in any official capacity I've always enjoyed our talks and admired your integrity! My examiner, **Sebastian**, thank you for being patient as I chased after you for signatures over the years, I hope things go well for you in Uppsala. **Kristina**, sensible and steadfast, good choice for deputy head of department! **Örjan**, pedagogic and kind, sorry if I sometimes cluttered your workplace on the first floor! **Gergely**, thank you for accepting the position as a chair person for my defence. It's calming to know things will be in good hands! **Björn**, you've always been cheerful and pleasant when I've met you. Climbing up the beerclub ladder by drinking cola every day is cheating, though! **Gisela**, I will never forget when you doubted my ability to sit in a flat-footed squat and challenged me to do so in front of a very bewildered Japanese bouncer. Turns out you were also able to do it! The bouncer remained unimpressed, though. **Greger**, the PhD would not have been as enjoyable without you. What I've learned from half filled coffee mugs all over the beamline, as well as a certain Osaka hangover, is that you don't like finishing your drinks. **Giorgia**, happy to have had you as an office-mate, I could have wished for no better! It feels good to know that you are never far away! **Dimitra**, thank you for showing me around

the lab on my first day, although you were as unclear as to what I was supposed to do as I was. It seems it all worked out in the end! **Analia**, I can always count on you to have food, tea, and condiments at hand. Adding a bit of chopped leek really spruces up a cup of ramen during a beamtime nightshift! **Lucija**, I'm sorry I like the wrong kind of metal. I have enjoyed working with you regardless! **Adams**, the lab would collapse without you (at least the servers would), thanks for the help when the linux-commands refused to do my bidding! **Arpitha**, you are probably the most cheerful person I have ever met. It's amazing that someone can be so happy while refusing to eat cheese! **Padmini**, a lady with flawless taste in books and an amazing hand when it comes to baking. Keep on slaying it! **Andreas**, I will deeply miss you and your Machiavellian ways, never change. **Owens**, the fanciest man there is, I think you might have more pairs of shoes than I have socks, but maybe that says more about me... **Doris**, I've enjoyed working with you. Thank you for the support during the teaching! **Jonatan**, you'll be the new laser man when I'm gone, I believe in you! **Emil**, I feel that a chemist making beer is just one small step away from going full breaking bad. Hopefully not, though, as I've found your beer very tasty! **Gabrielle**, glad to see you stay after your masters. I'm sure things will go great during your PhD as well! **Johan**, happy to have you in the lab. You seem to be fitting in well already! **Julia**, you are always fun to talk to, by far my favourite iron lady! **Leona**, it was a wise choice not to walk back to ESRF with us after the fondue in Grenoble. We got lost... If you keep displaying such good judgement things will work out for you! **Beatrice**, **Amanda**, I hope your master projects go well! **Ulrika**, wish you the best, I hope you are enjoying your work in the lab! **Jessica**, life as a mom suits you well. Looking forward to seeing you back in the lab, though! **Filomena**, you are a fun person to be seated next to at a party. I don't remember what we spoke of (there was something about unicorns), but I remember enjoying it! **Katharina**, you made the best snacks for your game and drink evening! Sorry about burning the toast a bit, though! **Vaj**, my mood always improves when running into you. I hope I get to do so many more times! **Laras**, I will miss our little chats. You are definitely better than me at drawing things for pictionary... **Torbjörn**, good luck in your project! **Andrea**, your grumpy exterior does little to hide your heart of gold! The lab will certainly not be the same without you. **Taru**, you

quickly became an essential component around the lunch/coffee table! I hope the constant trips to Finland wont wear you out! **Masoud**, I hope your postdoc progresses as you'd hoped. Best of luck in the future! **Amke**, I'm proud to beat you to the finish line by 4 days. Lets ignore the fact that I started about 6 months before you did... **Szabolcs**, good luck with your project and I hope you enjoy your time in Uppsala. **Ann**, starting my day without talking nonsense to you by the coffee table is just not the same. If it were up to me I'd permanently ban you from leaving and visiting Malaysia for weeks on end! **Irena**, thank you for the constructive talks about tubulin. It will surely leave me more prepared for my defence! **Josh**, I shall miss your dry wit. Your insights into 3D-printing have also been appreciated! **Charles**, a pleasure to occasionally start my morning by running into you on the bus. Soon you'll be able to take your commute in peace! **Damasus**, we started our PhD journey at about the same time and you've been a comforting presence throughout! Good luck in your future endeavours! **Emelie**, almost finished as well now, just a last push and you've got it! **Ylber**, you've worn the beerclub mantle exceedingly well. I'm grateful you didn't assassinate your way to the throne. **Jens**, hanging out with you at beerclub was always fun - a shame I could not do it more often! **Hannah**, best of luck with the rest of your project! **Filippo**, I'm glad we finally got an Italian in the lab that recognizes the parts of Italy that I've visited as actually being Italy! **Bozidar**, always greeting with a smile when I meet you. I hope you'll enjoy your time here! **Swagatha**, Sweden grew more gray as you left for Japan. I swear I will visit you as soon as I can! **Cecilia**, you are always my go to confidant, before you left the lab and after! Lets plan something fun once all this is over! **Tinna**, I have not really been looking too closely at the labspace since you left, but I assume that in your absence it's nothing but smouldering ruins. I hope you're having a good time at Astra. Lets keep in touch! **Majo**, one day I still hope to do the Japanese dinner. If you ever stray towards Mölndal I hope we can meet up for the occasional fika! **Rajiv**, carrying on work on your project took a few turns! A lot has changed but thanks for getting me started! **Rob**, I hear that sincerity can be troubling for many a Brit, so brace yourself! You are greatly missed and I hope you'll give me a shout next time you're in Sweden! **Sarabi**, you have brightened many a beamtime and gloomy lab day! Keep on shining! **Valida**, thank you for all

that you do in the lab. Your paintings are amazing! **Lars**, having access to your workshop and your expertise have helped me greatly throughout my PhD. Thank you very much! **Bruno**, once you are working on a problem I fell confident that it will be solved. Thank you for all your hard work! **All** people in the HR, we have not interacted much on a day to day basis, but the wheels would not be turning without you! Shoutout to **Johanna** for all the help with my contracts! **And** of course a thank you to all the previous PhDs and postdocs who've been in Lundberg lab during my time here. You all helped make my PhD fun!

Thanks to all my friends and family outside of the lab, thank you for being patient during my sometimes less than stellar presence throughout my PhD, especially the last year! And lastly, **Kadin**. You have been an absolute rock throughout all my ups an downs during my last years finishing up my degree. For that and many more things I will be eternally grateful! I love you.

Publications

This thesis consists of the following research papers:

PAPER I: Greger Hammarin*, **Per Börjesson***, Rajiv Harimoorthy, Guo Chen, Peter Berntsen, Per O. Widlund, Christer Stoij, Helena Rodilla, Jan Swenson, Gisela Brändén, Richard Neutze "**No Observable Non-Thermal Effect of Microwave Radiation On The Growth Of Microtubules**" Manuscript. To be submitted.

PAPER II: **Per Börjesson**, Greger Hammarin, Douglas Jutsell Nilsson, Christer Stoij, Thomas Hammarström, Richard Neutze "**Influence of Oscillating Electric Fields on the Growth of Microtubules**" Manuscript.

PAPER III: Greger Hammarin, **Per Börjesson**, Rajiv Harimoorthy, Alexandr Nasedkin, Christer Stoj, Daniel Sarabi, Giorgia Ortolani, Ana Diaz, Viviane Lutz-Bueno, Roberto Appio, Jan Swenson, Andreas Menzel, Gisela Brändén, Richard Neutze "**Microwave Induced Orientation Perturbations Of Microtubules**" Manuscript. To be submitted.

PAPER IV: **Per Börjesson**, Greger Hammarin, Juncheng E, Vajradhar Acharya, Mohammad Vakil, Raphael de Wijn, Lucija Ostojic, Daniel Sarabi, Peter Dahl, Richard Bean, Johan Bielecki, Huijong Han, Marco Kloos, Diogo V. M. Melo, Abhisakh Sarma, Tokushi Sato, Adrian Mancuso, Gisela Brändén, Richard Neutze "**Coherent Diffractive Imaging Studies of Microtubules Using Megahertz Data-Collection**" Manuscript

*These authors contributed equally to the study.

Papers that I have contributed to but are not included in this thesis:

PAPER VI: Petra Båth, Analia Banacore, **Per Börjesson**, Robert Bosman, Cecilia Wickstrand, Cecilia Safari, Robert Dods, Swagatha Ghosh, Peter Dahl, Giorgia Ortolani, Tinna Björg Ulfarsdottir, Greger Hammarin, María José García Bonete, Adams Vallejos, Lucija Ostojić, Petra Edlund, Johanna Barbara Linse, Rebecka Andersson, Eriko Nango, Shigeki Owada, Rie Tanaka, Kensuke Tono, Yasumasa Joti, Osamu Nureki, Fangjia Luo, Daniel James, Karol Nass, Philip J M Johnson, Gregor Knopp, Dmitry Ozerov, Claudio Cirelli, Christopher Milne, So Iwata, Gisela Brändén, Richard Neutze "**Lipidic Cubic Phase Serial Femtosecond Crystallography Structure of a Photosynthetic Reaction Centre**" Acta Crystallogr D Struct Biol. 2022 Jun 1;78(Pt 6):698-708.

PAPER VII: Swagatha Ghosh, Doris Zoric, Peter Dahl, Monika Bjelcic, Jonatan Johannesson, Emil Sandelin, **Per Börjesson**, Analia Banacore, Petra Edlund, Oskar Aurelius, Mirko Milas, Jie Nan, Anastasya Shilova, Ana Gonzalez, Uwe Mueller, Gisela Brändén and Richard Neutze "**A Simple Goniometer Compatible Flow-Cell for Serial Synchrotron Crystallography**" Submitted to Journal of applied crystallography. Revisions, awaiting resubmission.

PAPER VIII: Robert Bosman, Giorgia Ortolani, Swagatha Ghosh, Daniel James, **Per Börjesson**, Greger Hammarin, Tinna Björg Úlfarsdóttir, Tobias Weinert, Florian Dworkowski, Tomizaki Takashi, Jörg Standfuss, Gisela Brändén, Richard Neutze "**Structural Basis For the Prolonged Photocycle of Sensory Rhodopsin II Revealed by Serial Synchrotron Crystallography**" Submitted to Nature Communications. Revisions, awaiting resubmission.

PAPER IX: Giorgia Ortolani, Robert Bosman, Lucija Ostojic, Tinna Björg Úlfarsdottir, Swagatha Ghosh, Daniel James, Jack

B. Greisman, Kevin M. Dalton, Greger Hammarin, **Per Börjesson**, Tobias Weinert, Florian Dworkowski, Takashi Tomizaki, Doeke R. Hekstra, Joerg Standfuss, Gisela Brändén, Richard Neutze "**Serial Synchrotron Crystallography Structure Of The Sensory Rhodopsin II: Transducer Complex**" Manuscript.

PAPER X: Giorgia Ortolani, Robert Bosman, Lucija Ostojic, Jack B. Greisman, Kevin M. Dalton, Adams Vallejos, Tinna Björg Úlfarsdottir, Swagatha Ghosh, Daniel James, Greger Hammarin, **Per Börjesson**, Tobias Weinert, Florian Dworkowski, Takashi Tomizaki, Joerg Standfuss, Doeke R. Hekstra, Gisela Brändén, Richard Neutze "**Serial Crystallography Structure Of The Light-Activated Sensory Rhodopsin II: Transducer Complex**" Manuscript.

PAPER XI: Daniel Sarabi, Robert Bosman, Lucija Ostojic, Swagatha Ghosh, Giorgia Ortolani, Matteo Levantino, Martin Nors Pedersen, Mathias Sander, Petra Båth, Greger Hammarin, Robert Dods, **Per Börjesson**, Cecilia Safari, Michael Wulff, Gisela Bränden, Richard Neutze "**Time Resolved X-Ray Solution Scattering Observations Of Light Induced Structural Changes In Sensory Rhodopsin II**" Manuscript.

PAPER XII: Cecilia Safari, Swagatha Ghosh, Rebecka Andersson, Jonatan Johannesson, Petra Båth, Robert Bosman, Peter Dahl, Eriko Nango, Rie Tanaka, Elin Dunevall, **Per Börjesson**, Owens Uwangue, Doris Zoric, Greger Hammarin, Matthijs Panman, Emil Svensson, Giorgia Ortolani, Tomoyuki Tanaka, Takehiko Tosha, Hanae Takeda, Hisashi Naitow, Toshi Arima, Ayumi Yamashita, Michihiro Sugahara, Takanori Nakane, Osamu Nureki, So Iwata, Richard Neutze & Gisela Brändén "**Time-Resolved Serial Crystallography to Track the Dynamics of Carbon Monoxide in the Active Site of Cytochrome C Oxidase**" Manuscript.

Contribution report

PAPER I: I purified protein, helped design and build the experimental setup, collected data, and helped analyse data and write the manuscript.

PAPER II: I purified protein, designed and contructed the device used to deliver high voltage fields, designed and built the experimental setup, collected and analyzed data, and helped write the manuscript.

PAPER III: I purified protein, participated in the experiment beamtime, and helped write the manuscript.

PAPER IV: I purified protein, applied and prepared for the beamtime, participated in the experiment beamtime, analyzed data, and helped write the manuscript.

Abbreviations

Here follows a list of the different abbreviations used in this thesis.

EF	**E**lectric **F**ield
HV	**H**igh **V**oltage
TTF	**T**umor **T**reating **F**ield
MT	**M**icro**T**ubules
GTP	**G**uanosine-5'-**T**ri**P**hosphate
GDP	**G**uanosine-5'-**D**i**P**hosphate
MAP	**M**icrotubule-**A**ssociated **P**rotein
XFEL	**X**-ray **F**ree **E**lectron **L**aser
LEG	**L**ow-**E**mittance **G**un
BC	**B**unch **C**ompressor
SASE	**S**elf-**A**mplified **S**pontaneous **E**mission
SAXS	**S**mall **A**ngle **X**-ray **S**cattering
WAXS	**W**ide **A**ngle **X**-ray **S**cattering
OD	**O**ptical **D**ensity
TR-XSS	**T**ime **R**esolved **X**-ray **S**olution **S**cattering
SHV	**S**afe-**H**igh **V**oltage

Contents

Chapter 1

Introduction

The work presented in this thesis centres around electric fields and their effect on the structure and dynamics of microtubules. The following introduction seeks to explain concepts and techniques used to investigate these effects.

1.1 Electric Fields

Perhaps the simplest example of an electric field is of two differing (negative and positive) charges separated in space. Although the charges do not touch, they still produce an effect on each other. The volume where this effect is present is referred to as an electric field. The strength of an electric field is determined by the strength of the differing charges, as well as the distance between them. Closer charges will produce higher fields. The standard unit for measuring an electric field is volt per meter (V/m) [1, 2].

1.1.1 Effect of Electric Fields on Proteins

Any charge within an electric field will be subjected to a force directing it to its corresponding pole (negative charge towards positive pole, *vice versa*). This phenomenon can result in the movement of charged particles within a field or rotation and linearization of dipoles (molecules or systems with a charge separation). The possibility of more complex effects induced on big biomolecules has long been discussed. Herbert Fröhlich, a German born Brittish physicist, proposed in 1968 that biological molecules could

store energy in vibrational modes accessed by certain frequencies [3, 4]. While this proposal was theoretical in nature, it indicates possible interactions of biological systems with electrical fields. Many practical studies on biological effects caused by electrical fields have since been performed. Some of these studies have shown direct effects from electric fields on biological systems, while other studies attribute observed effects to thermal heating caused by the electric fields [5–8].

More specific biological entities which could potentially be affected by electric fields are proteins. Proteins often have nonzero electric dipole moments and are thus likely to change their orientation when subjected to an electric field [9, 10]. Furthermore, direct effects of electrical gradients on protein function have been observed, such as the case with so-called voltage sensors. Voltage sensors are usually domains of a protein sensitive to differences in electric potential. They often trigger conformational changes in ion channels or transporters, activating them [11–14]. Furthermore, a study performed by Hekstra et al showed that it is possible to induce structural motions within a protein with no known functional voltage dependence by subjecting a protein crystal to a high-voltage electrical field [15]. It therefore seems clear that under many circumstances proteins are affected by electrical fields. Could then externally applied man-made electric fields promote changes in proteins found in human cells, which in turn could effect cell metabolism or function of said cells? Different studies have been performed trying to determine the effect of lower voltage, high frequency alternating fields (the polarity of the electric field inverses periodically), many of these with a focus on possible pathological effects with toxicological endpoints, such as cancer.

1.1.2 Electric Fields and Public Health

While no scientific consensus has been reached, concerns regarding possible detrimental effects of high frequency fields remain in the public eye, perhaps most recently exemplified by the concern regarding 5G-expansion and its potential effect on biological systems. In a review published by K. Karipidis et al [16]. it is concluded that, while many studies have been performed in the area, it is difficult to draw any strong conclusions as to

the effect of 5G-frequencies on biological systems. The reasons listed are poorly conducted studies in terms of experimental design and control, as well as reported bioeffects generally not being independently replicated. Their takeaway is that more studies need to be performed in the area. Similar conclusions are drawn in a review by I. A. Cotgreave when he investigates biological stress responses induced by radiofrequency emissions given off by cell phones [17]. Many other man-made electric fields have also been investigated including radiation given off by power lines and radio transmitters. [18–22] Although no pathological effects have been clearly observed, guidelines by the International Commission on Non-Ionizing Radiation Protection (ICNIRP) were updated in 2020. These guidelines, viable for frequencies between 100kHz to 300GHz, state that in some circumstances electric fields can give rise to electroporation (a change in the permeability of cell membranes) or more commonly, temperature elevation as a result of microwave heating (microwaves frequencies ranging between 1-1000 GHz). [23, 24]

1.1.3 Usage of Electric Fields in Cancer Treatment

The effects of electric fields of lower frequencies on biological systems have also been investigated. In 2004, Kirson E et.al discovered that low-voltage electrical fields (1-3 V/cm) in the frequency range of 100-300 kHz could generate a significant inhibitory effect on proliferating cancer cells undergoing division [25, 26]. The studies suggest two mechanisms of action behind the observed effects. The first argument states that part of the effect could be due to inhibitory action on tubulin binding to polymerizing microtubules under the effects of an electric field. The argument stated that an externally applied electric fields could misalign the tubulin with respect to the microtubules, slowing down polymerization. The second argument is that an electric field acting on a dividing cell is amplified in the furrow of the cell due to the hour-glass shape of the cells mid division. This amplification could cause charged and polar entities within the cell to be pulled towards the furrow, thus interfering with cytokinesis. Since the discovery of these Tumour Treating Fields (TTFs), studies have been performed to determine the exact mechanism behind its efficiency. In a study performed by Tuszynski et al. an argument is made that the effects

of tumour treating fields on tubulin dipoles is not significant enough to affect polymerization significantly [27]. They go on to say that microtubules and tubulin can interact with electromagnetic forces in a number of ways but that determining the specifics of these effects are not trivial and require careful examination. The exact mechanism of action behind tumour treating fields is yet to be precisely determined and more work in the area is required in order to further increase the efficiency of this form of cancer treatment [28]. Microwave frequencies can also be used for cancer treatment. This method, however, relies on heating the area close to a tumour to temperatures usually above 40°C, creating a hostile environment for the cancer cells. This type of microwave induced hyperthermia is often used in combination with other cancers treatments, such as radiation therapy or chemotherapy [29, 30].
This thesis seeks to add to the discourse on health effects of electrical fields, specifically by investigating the effects of electric fields on microtubules. Microtubules are protein structures common throughout the body and essential for cell division and other cell functions. [31] Their constituents, the smaller protein tubulin, are highly polar, making the microtubule polar as well. The prevalence and importance of microtubules throughout the body, as well as their dipolar properties, make them an interesting target when investigating biological effects brought on by oscillating electric fields. [32–36]

1.2 The Cytoskeleton and Microtubules

1.2.1 The Cytoskeleton

The cytoskeleton, depicted in figure 1.1, is an integral part of a eukaryotic cell. It helps the cell maintain its shape and performs multiple functions including organizing the organic molecules in the cytoplasm, aiding in cell movement, aiding in internal transport of intracellular structures, and separation of the chromosomes during cell division. The cytoskeleton consists of protein filaments capable of reforming themselves based on the current needs of the cell, making the cytoskeleton a dynamic and flexible structure. One of the protein filaments present in the cytoskeleton are the microtubules [31, 37].

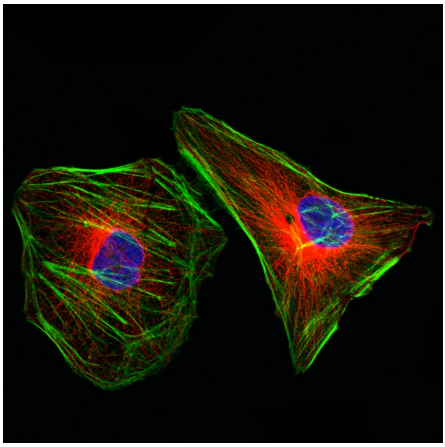

Figure 1.1: Image of a cancer cell stained for cytoskeletal proteins seen in red and green. Image taken from [38].

1.2.2 Microtubules

Microtubules, along with actin filaments and intermediate filaments, are one of the three major components of the cytoskeleton. They are tubular with an outer diameter of about 25 nm and are composed of a protein called tubulin. Tubulin is a globular heterodimer protein made from two similar polypeptides, α- and β-tubulin, each with a molecular weight of about 55 kDa and each with a primary structure that is 41% identical to the other [39]. These dimers polymerize into linear protofilaments that, in turn, assemble in groups of usually 13 around a hollow core to form the microtubule (figure 1.2), while 13 is considered to be the most common amount of protofilaments in a microtubule, microtubules with between 4 to 40 protofilaments have also been observed *in vivo*, with different properties associated with them [40, 41]. Different isotypes of α- and β-tubulin have been found in a variety of organisms. These isotypes, while very similar in structure, usually perform slightly differently. These slight differences can change a variety of properties within microtubules, such as their stiffness, their propensity for depolymerization, their likelihood to interact with other proteins, *etc*. Different tubulin isotypes are thought

to allow for microtubule specialization, promoting the unique function of specialized tissues [42–44].

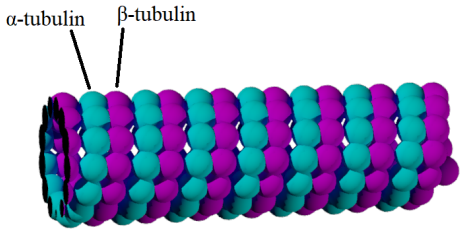

Figure 1.2: Crossection of microtubule, illustrating the 13 protofilaments as well as the α- and β-tubulin dimers.

Polymerization can only occur if the tubulin binds to two guanosine-5'-triphosphate (GTP) molecules, one for each dimer subunit. The GTP bound to the α-tubulin remains stable, whereas the GTP bound to the β-tubulin hydrolyses into guanosine-5'-diphosphate (GDP) during, or shortly after, the polymerization. Initial polymerization of tubulin into microtubules may occur spontaneously; however, oligomers containing just a few tubulin dimers are unstable and will most often collapse. Since early tubulin interactions are unlikely to give rise to the more stable microtubules, a high concentration of tubulin dimers is usually needed in order for spontaneous polymerization to occur *in vitro*. In the cell, microtubule-associated proteins (MAPs) accelerate the addition of tubulin to a growing oligomer or strengthen the tubulin-tubulin bonds, aiding microtubule polymerization [45–49]. Once the formation of longer, more stable, microtubules commences, an initial region of non-hydrolysed GTP will exist in the growing end of the microtubules, stabilizing them. If no further binding of tubulin occurs, the GTP will soon hydrolyse into GDP, weakening the binding affinity of adjacent molecules by inducing a structural change in β-tubulin and thus increasing the probability that the microtubule will depolymerize and release tubulin dimers [50]. Once depolymerized, the

β-tubulin can exchange its GDP for a fresh GTP molecule, leaving the tubulin dimer free to undergo another round of polymerization. Hydrolysis of GTP into GDP and the subsequent release of GDP to create space for a fresh GTP molecule on the β-subunit constitute what is referred to as dynamic instability, illustrated in figure 1.3. This dynamic instability is an essential property of microtubules and causes individual microtubules to alternate between cycles of growth and shrinkage. Furthermore, because α- and β-tubulin arrange linearly during polymerization, each end of the microtubule behaves somewhat differently. The microtubule end capped with β-tubulin, the plus end, is more dynamic. The less dynamic α-tubulin capped end, the minus end, is usually anchored in a microtubule organizing structure, such as a centerosome, in the natural environment of the cell. [31, 45–48, 51]

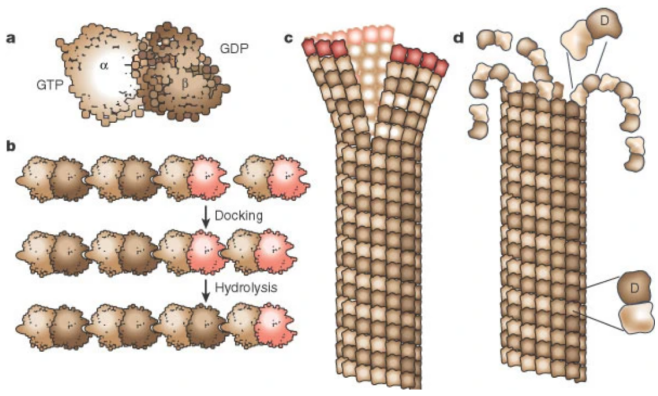

Figure 1.3: Plus end of a microtubule. **a**: an α- and β-tubulin dimer with bound GTP and GDP. **b** protofilaments docking and undergoing GTP hydrolysis. β-tubulin in pink. **c** growing end of microtubule **d** microtubule plus end depolymerizing as a result of GTP hydrolyzation. Image taken from [52]

1.2.3 Microtubules and Cancer

During cell division, an essential role of microtubules is to help split the chromosome pairs of a mother cell into two identical sets of chromosomes

for the resulting daughter cells. This key role in cell division has made microtubules an important target for many anti-cancer drugs. These drugs suppress microtubule dynamics, often hindering cell division and in some cases leading to apoptosis. Significant research has gone into both utilizing microtubules as a target for anticancer drugs as well as detecting and analysing mechanisms of resistance to some microtubule binding pharmaceutical agents [53–56]. One specific anticancer drug that was used in the making of this thesis, specifically in **paper 4**, is paclitaxel. Paclitaxel, also known as taxol, was first discovered by Monroe E. Wall and Mansukh Wani. In 1971 they extracted taxol from *Taxus brevifolia*, or Pacific yew, and suggested it as a possible anti-leukemic and anti-tumour agent [57]. It has since been used as a anti-cancer agent, successfully helping treat a variety of cancers [58–60]. Paclitaxel binds to the β- subunit of the tubulin dimer and stabilizes the microtubules by counteracting the effects of GTP hydrolization, hindering depolymerization [61–63], which in turn affects the flexible dynamic instability needed for normal cell division. Apart from its use in cancer treatment paclitaxel has been used to stabilize microtububles and tubulin assemblies in order to ease the structural study of both microtubules and its constituents, the α- and β-tubulin [64–66].

The dynamic instability of microtubles is one of the keys to cell division and development. Studying potential external factors impacting microtubule formation could provide insight into the performance of the cell under different environments and also aid in the development of new and improved anti-cancer drugs.

1.2.4 Microtubules and Electric Fields

Both α- and β-tubulin have high electrical dipole moments that, when combined, result in a high dipole moment for the resulting heterodimer as well. The directionally ordered fashion in which microtubules are built up by the heterodimers in turn gives the microtubules a significant electric dipole [67, 68].

Highly speculative papers have been released, such as works by Hameroff, Penrose and Craddock, that hypothesize that microtubules may play an essential role in consciousness and intellect by processing information in

a "computer-like" fashion. [69–71]. With little experimental studies performed to support such claims, they remain of limited practical value, but point to potential interesting aspects of microtubules and their potential interaction with electrical fields.

In this thesis the effect of alternating electric fields of different frequencies on microtubules has been studied. As briefly mentioned in section 1.1, it has been theorized that biomolecules, such as the microtubules, could be able to store energy in vibrational modes [4]. Theories in the same vein, claiming that vibrations in microtubules could be utilized in the cell in order to facilitate mass transport and communication have been suggested by Pokorný et al [72]. This was countered by a theoretical study performed by Kenneth R. Foster et al. which claims that any such vibrational processes would be dampened by the viscosity of the surrounding liquid (mostly water) [73]. Pokorný goes on to suggest that a "slip boundary" condition where a thin layer of adsorbed molecules on the surface of microtubules might allow for a decreased dampening effect of the viscous surroundings, thus still allowing for microtubule vibration effects [74]. However, experimental proof for this effect has yet to be seen.

Water, with its relatively high permittivity, will oppose any external electrical field acting on it to varying degrees depending on its temperature and the frequency of the applied electric field [75–77]. The possibly significant dampening of the bulk solution on the vibrations of microtubules, as well as the low propagation of electric fields into a aqueous media, will cause any effects on the target microtubules from applied electric fields to be quite vague and difficult to detect. In this thesis, the effect of oscillating electric fields on the structure and polymerization of microtubules are probed using both X-ray and light scattering.

1.3 Radiation Sources and Diffraction

When discussing radiation and diffraction, it seems pertinent to start with discussing the electromagnetic spectrum. The electromagnetic spectrum refers to the distribution of wavelengths of electromagnetic radiation present throughout the universe. Visible light makes up a portion of this

spectrum with wavelengths ranging from about 380 nm (violet light) to 700 nm (red light) [78, 79]. While not detectable by the human eye, the electromagnetic spectrum continues above 700 nm and enters sub-spectra of longer wavelength radiation, including regions such as microwave radiation and radio waves. Similarly, the spectrum stretches below 380 nm and includes regions such as X-rays and gamma-rays. [79] An overview of the electromagnetic spectrum is shown in figure 1.4.

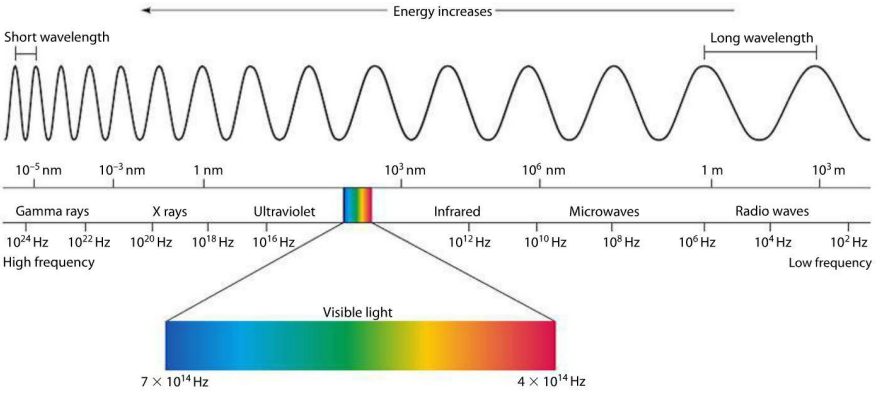

Figure 1.4: The electromagnetic spectrum, illustrated above, is the collective name for the wide range of photon wavelengths that can be emitted by electrons. Image taken from [80].

A wave of electromagnetic radiation may interact with elements in its path, potentially giving rise to a number of phenomena, including diffraction. In classical physics, Dutch mathematician Christian Huygens first explained diffraction by imagining that every part of a parallel wave was the source of new radiation of the same phase and frequency [81]. An illustration of this principle is shown in figure 1.5. The points on a parallel wave (a finite number of points illustrated, though in actuality the amount is infinite) produce circular waves of identical phase and frequency. Due to destructive interference, most parts of these circular waves cancel each other out, while the surviving amplitudes create a new, parallel wave front. If these parallel waves were to hit an obstacle, in figure 1.5 represented

as a slit, the circular waves created by the wave front will no longer cancel out to the same extent. The waves created by the wave front closest to the edge of the slit are instead allowed to propagate outwardly in a way no longer parallel to the original waves. This is referred to as diffraction [81, 82]. Worth noting is that Huygens principle, while elegant in its simplicity, fails to completely describe diffraction in its entirety. Revised, more accurate, models now exist that better describe diffraction of electromagnetic waves [83]. Huygens original description, however, remains useful as an intuitive model.

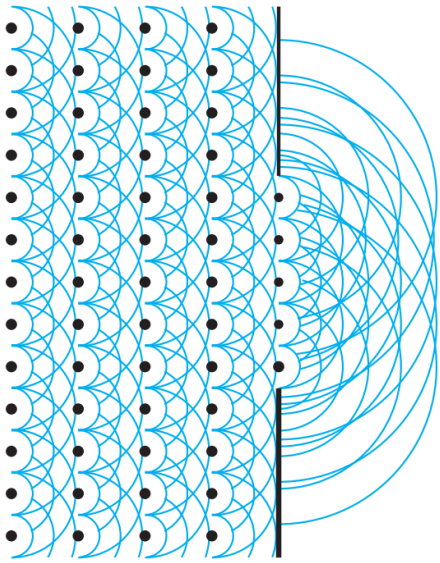

Figure 1.5: Illustration of Huygen's principle. Each point of the wave front gives rise to another wave of same frequency and phase, thus propagating the wave. Picture from [82].

Diffraction is thus waves of light bending around an obstacle in a way that is dependent on the wavelength of the radiation, as well as the shape and size of the obstacle [84, 85]. For example, consider another slit experiment wherein parallel waves of electromagnetic radiation hit a slit of similar width to their wavelength, and the resulting diffracted radiation is then registered by a parallel detector (figure 1.6). The radiation will

diffract outward in a spherical pattern away from the slit and hit the detector as roughly described by the orange intensity pattern in figure 1.6. The diffracting waves will interfere constructively (crests of two or more waves combine and result in a wave with higher amplitude), destructively (a crest of one wave combines with the trough of another, cancelling each other out), or in a combination of the two. Thus, parts of the detector will register higher intensities, while others will register no intensity at all due to the destructive interference [84–86]. A more detailed explanation of the relationship between diffraction patterns and the characteristics of corresponding diffraction-causing objects will follow later in this chapter. For now, it can simply be stated that it is possible to invert a diffraction pattern to recover information about a diffracting object.

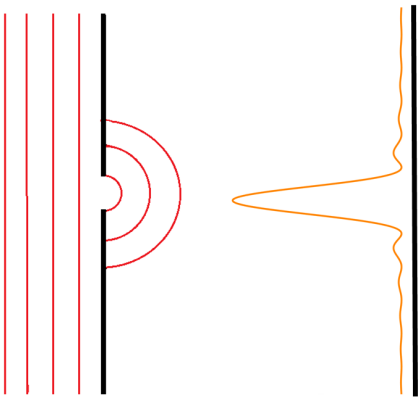

Figure 1.6: Illustration of parallel electromagnetic radiation (visualized as red lines to the left of the image) diffracting as it hits a slit of approximately the same size as the wavelength incident radiation (diffracting radiation visualized as half circles spreading to the right of the slit). The orange line illustrates the resulting detected intensities.

The information content from diffraction is maximal when an electromagnetic wave interact with objects roughly the same size as the radiation wavelength. Thus, if one is interested in looking at proteins, where the distance between two amino acids are at the level of around 4 Å, [87] the use of electromagnetic radiation in the X-ray regime (about 1 to 100

Å [88]) is required. X-ray radiation of these energies can be generated in many ways including using state of the art particle accelerators, namely X-ray Free Electron Lasers (XFELs) or synchrotrons.

1.4 XFELs and Synchrotrons

XFELs and Synchrotrons are able to accelerate electrons to near-light-speed. The high-speed electrons are made to go through periodic structures of dipole magnets, called undulators, which cause the electrons to oscillate and release radiation in the X-ray regime [89]. While both XFELs and synchrotrons produce X-rays, the X-rays they produce have different characteristics depending on their source. In XFELs electrons are emitted from a Low-Emittance Gun (LEG) by way of a picosecond laser, then accelerated in a short linear accelerator before being compressed using Bunch Compressor (BC) magnets. The electrons proceed to enter a long linear accelerator, sometimes kilometres in length, until they reach near-light-speeds. The electrons then oscillate as they pass through a section of undulators, releasing radiation as they do (figure 1.7a). The released radiation interacts with the electrons as they oscillate, slowing some of the electrons down and accelerating others. This so-called Self-Amplified Spontaneous Emission (SASE) causes an accelerated electron bunch to organize into thinner sections of microbunches that all oscillate in unison, resulting in very short coherent bursts of X-ray radiation [90, 91].
In Synchrotrons, on the other hand, electrons are first accelerated using a small linear accelerator, usually called an electron gun or linac. After the linac, the electrons are usually (but not in all cases) fed into a relatively small booster ring, where they are further accelerated prior to being injected into a large storage ring where they orbit through a system of magnetic field devices. These devices can bend or wiggle the electrons, producing radiation in a wide range of wavelengths. There are also undulators that allow for bright, highly collimated light to come out of different beamlines placed along the storage ring. See figure 1.7b for illustration.

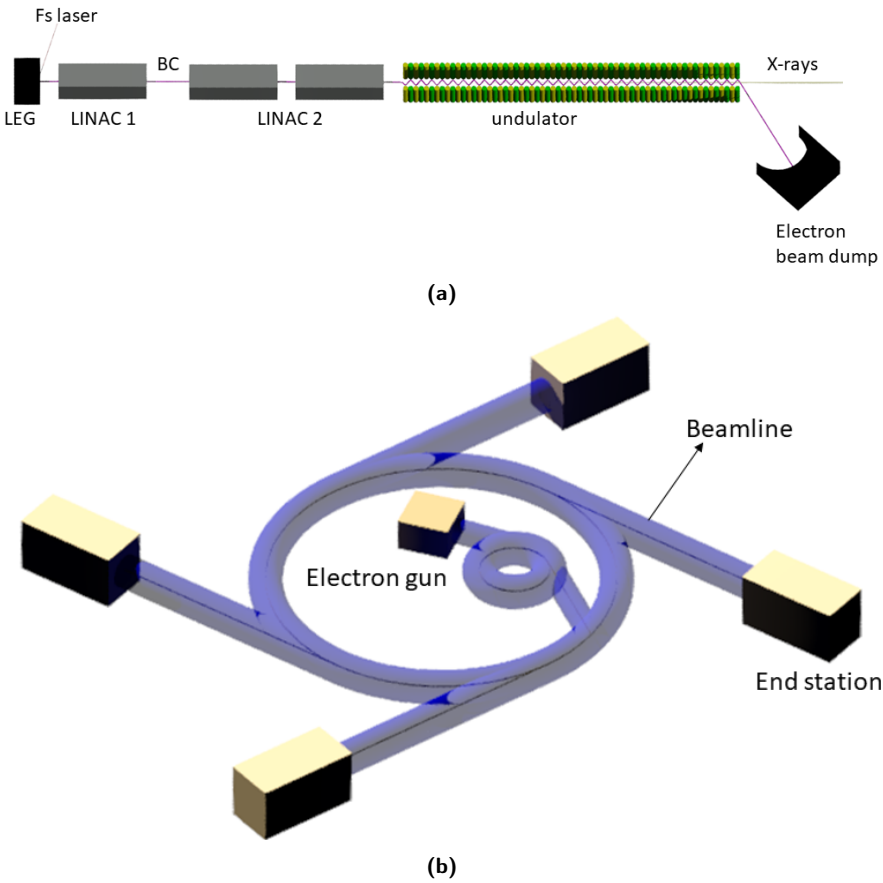

Figure 1.7: a) Illustration of an XFEL. b) Illustration of a synchrotron facility. A typical beamline is also depicted showing an end station, which usually contains an optics cabin, experimental cabin, and a control room.

XFELs create very short bursts of radiation, in the timescale of femtoseconds, and they also have a higher brilliance (a high photon flux with a low divergence) when compared to a synchrotron. While XFELs might seem superior to synchrotrons at first glance, they both have their uses. If one is interested in capturing very fast (in the range of femtoseconds) molecular dynamics, XFELs are more able to create a series of diffraction patterns illuminating the motions of a molecular process. However,

synchrotrons are suitable when looking at slower molecular movements (micro- to milliseconds). Furthermore, the lower brilliance of synchrotrons allow for multiple X-ray exposures of a sample before it starts to break down due to radiation damage, which might be of use when trying to avoid damage to both sample and sample setup. In short, both XFELs and synchrotrons are powerful tools when uncovering structures and dynamics of proteins in different environments. [90–94] During the work presented in this thesis, both XFELs and synchrotrons have been used in order to uncover structural characteristics of microtubules in different environments. The choice between the two technologies was dependent on the type of study performed and the type of setup used. Availability of radiation facilities also played a part.

1.4.1 SAXS and WAXS

Small Angle X-ray Scattering (SAXS) and Wide Angle X-ray Scattering (WAXS) refer to two different types of scattering studies. In a SAXS-study, one tends to want to retrieve structural information from relatively large structures, in the range of a few nanometers up to a few hundred nanometers, since these larger structures tend to scatter x-ray light at relatively small angles [95]. Smaller structures, on the other hand, tend to scatter x-ray light at wider angles, thus WAXS-studies are applied when probing for information on structures or sub-structures in size ranges lower than those appropriate for SAXS-studies [96, 97]. In **paper 4** we tried to determine structure of microtubules in a thin liquid jet, and in **paper 3** we combined SAXS and WAXS to look for structural changes in microtubules when subjected to electric fields in the GHz-range.

1.5 Scope of Thesis

This thesis investigated the effects of electrical fields on microtubule function and structure. Microtubules in solution were probed using either light scattering or X-rays while subjected to an oscillating electric field. It was also attempted to determine the structure of microtubules in solution using an X-ray laser.

In **paper 1** we used light scattering to determine if electric fields with microwave frequencies had any effect on the rate of polymerization of microtubules. It was determined that any effects induced during polymerization was a result of the samples thermal history.

In **paper 2** light scattering was again used, this time to probe microtubule polymerization subjected to high voltage fields in the frequency range of TTFs. A slight difference in polymerization speed could be seen for microtubules subjected to fields with a frequency of 147 kHz.

In **paper 3** we subjected a solution of pre-polymerized microtubules to electric fields in the microwave domain and probed the solution using X-rays. The results showed that the fields cause microtubules to align parallel to the direction of the fields, but no structural changes within the microtubules themselves could be detected.

In **paper 4** we used a gas dynamic virtual nozzle to focus a solution of paclitaxel stabilized microtubules into a thin jet. The jet was probed using an X-ray laser and diffracted images were collected as a basis for reconstructing the microtubule structure. The analysis of the data proved taxing and more work needs to be done before a good reconstruction is possible.

Chapter 2

Method

This chapter seeks to explain methods and concepts utilized while conducting the experiments that resulted in **paper 1-4**.

2.1 Tubulin Purification

The tubulin purification procedure described below was adapted from a method published by Mirco Castoldi and Andrei V. Popov in 2003 [98]. It uses the inherent ability of tubulin to polymerize into microtubules or depolymerize depending on the environment they are in. Through a series of cold and warm centrifugation steps where the tubulin were in a depolymerized, or polymerized state respectively, it was possible to extract the protein from its source.
Tubulin was extracted and purified from porcine brains provided fresh after slaughter (approximately 40 min) by Dalsjöfors Meat AB. The brains were transported from the slaughterhouse to the laboratory in ice-cold PBS (Phosphate Buffered Saline, 20 mM Na-phosphate, 150 mM NaCl, pH 7.2) to slow down protein degradation. Once in the lab the brains were cleaned from blood and cut into smaller chunks. An equal amount of cold (4°C) DB (Depolymerization Buffer, 50 mM MES, 1 mM $CaCl_2$, pH 6.6) was added to the brain chunks together with protease inhibitor (Protease Inhibitor cocktail, 5 ml from Sigma Aldrich), and the mixture was homogenized in a blender until smooth (about 60 s). The homogenate was then centrifuged with a JLA 8.1 (Beckman Coulter) centrifuge rotor at 7000 rpm for 20 min at 4^oC. The supernatant was saved and placed into a Beckman JA 14 rotor and centrifuged at 14000 rpm for 80 min at 4°C. The

tubulin containing supernatant was mixed with warm (37°C) HMPB (High Molarity PIPES Buffer, 1 M PIPES, 20 mM EGTA, 10 mM MgCl, pH 6.9) and glycerol in a 1:1:1 ratio. ATP and GTP were added to the mixture to a final concentration of 1.5 mM and 0.5 mM respectively. The mixture was quickly heated to 30°C by holding the container under a stream of hot water and the container was subsequently placed in a 37°C water bath for 60 min to allow for tubulin polymerization. After the polymerization was completed the microtubule containing solution was centrifuged in a Beckman Ti45 rotor at 44000 rpm for 30 min at 37°C. The pellet from this centrifugation was collected and resuspended in DB. This suspension was placed on ice for at least 30 min. Once microtubules had time to depolymerize the mixture was centrifuged in a Beckman Ti70 rotor at 30000 rpm for 30 min at 4°C. The supernatant from this centrifugation step was again pooled with heated HMPB and glycerol in a 1:1:1 ratio. Once ATP and GTP were added to a final concentration of 1.5 mM and 0.5 mM respectively, the solution was put in a 37°C water bath to polymerize for 30 min. After the polymerization the solution was once again centrifuged in a Beckman Ti45 rotor at 44000 rpm for 30 min at 37°C. Pellets were again collected, resuspended in DB, and then put on ice for at least 10 min. Resuspended solution was subsequently centrifuged in a Beckman Ti70.1 rotor at 60000 rpm for 30 min at 4°C. The final tubulin concentration was determined at A280 using an extinction coefficient of 115000 after which the protein was snap frozen using liquid nitrogen. A flowchart featuring the extraction procedure can be seen in figure 2.1.

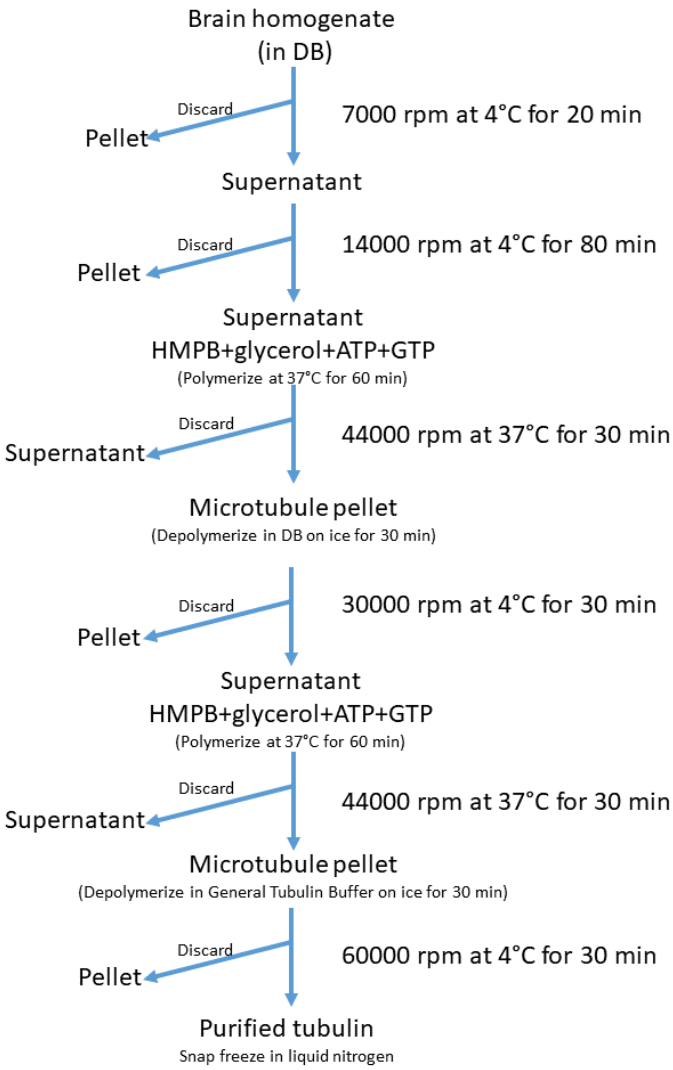

Figure 2.1: Flowchart of the tubulin preparation.

2.2 Light Scattering

In **paper 1** and **paper 2** we measured the polymerization of tubulin into microtubules via light scattering. The process of tubulin polymerization into microtubules is typically divided into phases. Initially, free tubulin in solution will aggregate and form protofilaments, which in turn aggregate and form bidemensional sheets. At a certain size, once the sheets fold into tubes, additional tubulin binding to these bidimensional sheets will become thermodynamically favourable and further development into a full-fledged microtubule is possible. These stable bidimensional sheets are referred to as critical nuclei and the creation of these nuclei mainly take place during what is called the "nucleation phase" [99, 100]. Once enough stable nuclei are present, free tubulin will polymerize onto these nuclei, making them longer. This phase is referred to as the "elongation phase" [100, 101]. As these nuclei grow into full-fledged microtubules they will enter a phase where the growth of microtubules lies in balance with their collapse via the process of dynamic instability, further explained in chapter 1.2. The growth process of microtubules can be monitored using light scattering [101, 102]. As a molecule changes size and shape, so will it also change what wavelengths of light it scatters. As mentioned in section 1.3, larger molecules will generally scatter light with a longer wavelength [103]. Probing a tubulin sample using a wavelength of 310 nm or lower will result in significant scattering from tubulin dimers and buffer. Thus, a higher wavelength is more suitable when tracking microtubule polymerization as it avoids scattering from smaller molecules but still scatters from forming microtubules [102]. Incident light with wavelengths longer than 310 nm will mostly remain unscattered by background molecules. As microtubules increase in length and number, the optical density (OD) of the sample will increase and more light will scatter. See example in figure 2.2. In this thesis, light scattering tracking of microtubule polymerization was performed using a LED-light with a wavelength of 365 nm.

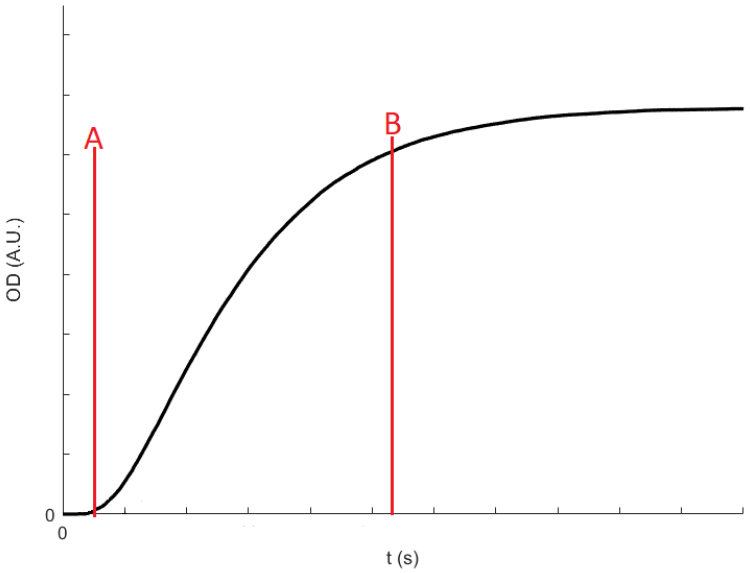

Figure 2.2: An illustration of the type of polymerization curve one would obtain via light scattering. As microtubules polymerize the turbidity of the solution increases and more light will be scattered. Before time point "A", the nucleation phase takes place, in this phase the nuclei are small enough not to scatter the probing light and will thus not contribute to an increase in OD. Between "A" and "B" we see the elongation phase, where an exponential increase in long microtubules scatter incident light, resulting in an overall increase in sample OD. After "B" the curve reaches a plateau, where a balance between the growth and collapse of the microtubules takes place resulting in no observable change in OD as time goes on.

2.2.1 Solution Scattering

As previously mentioned, it is possible to use a diffraction or scattering pattern in order to reconstruct the structure of a scattering object. This section will go more into depth on the theory of image reconstruction from scattering patterns originating from macromolecules in solution, so

called solution scattering.
Imagine a protein-buffer solution hit by an incident X-ray beam represented with the momentum vector $\vec{s_0}$, so that

$$|\vec{s_0}| = \frac{2\pi}{\lambda}. \tag{2.1}$$

where λ is the X-ray wavelength. Both the protein and the buffer consist of atoms and all these atoms have clouds of electrons orbiting them. One of these electron clouds will cause a small fraction of the X-ray beams passing through it to scatter at an angle 2θ resulting in the scattered X-ray $\vec{s}$ (figure 2.3).

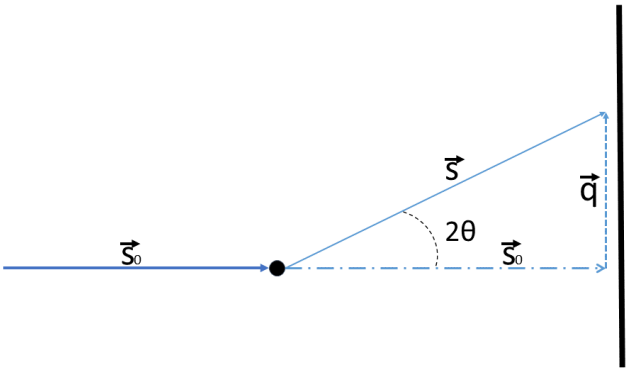

Figure 2.3: Incident X-ray beams $\vec{s_0}$ scatter on a sample at an angle 2θ resulting in scattered X-rays $\vec{s}$. A momentum transfer vector $\vec{q}$ is here the difference between vectors $\vec{s}$ and $\vec{s_0}$.

Assuming elastic scattering (no change in photon energy before and after scattering), one expresses a momentum transfer, $\vec{q}$ so that

$$\vec{q} = \vec{s} - \vec{s_0} \implies |\vec{q}| = \frac{4\pi sin(\theta)}{\lambda}. \tag{2.2}$$

In a protein many electron clouds will be present and there will thus be a need to sum the waves interacting with each electron cloud. If we

assume the electron clouds can be represented as spherically symmetric, this sum takes the form of an integral, as follows:

$$f(q) = 4\pi \int \rho(r) r^2 \frac{sin(qr)}{qr} dr \tag{2.3}$$

In equation 2.3 r designates the distance between diffracting points and $\rho(r)$ is the distance distribution function. When proteins are suspended in a solution their spatial orientation is usually random. This means that any X-ray beam hitting a sample will result in an intensity signal that is an average over all protein orientations. This is taken into account by using the Debye formula, which gives the intensity curve for a probed set of randomly oriented proteins [104, 105]

$$I(q) = \sum_i \sum_j f_i(q) fj(q) \frac{sin(qr_{ij})}{qr_{ij}} \tag{2.4}$$

where r_{ij} is equal to $|r_i - r_j|$ which is the distance between atom i and j. In a real-life setting one must also take into account the effect the solvent has on the total scattering of a protein solution. Taking this into account gives us an expression for the measured intensity from a protein scattering in solution:

$$I(q) = \left\langle \sum_i \sum_j (f_i(q) - \rho_s v_i)(fj(q) - \rho_s v_j) \frac{sin(qr_{ij})}{qr_{ij}} \right\rangle \tag{2.5}$$

where ρ_s is the scattering density of the solvent, v_i is the volume of solvent displaced by atom i, and the $\langle ... \rangle$ brackets represent an average over all orientations [104, 106]. This intensity scattering curve is the Fourier transform of the pair distance distribution function usually denoted $P(r)$, which carries information about the real distances between electron clouds in the probed sample, thus allowing for retrieval of information about the structure of a diffracting sample.

2.2.2 Coherent Diffractive Imaging

In traditional X-ray microscopes, when utilized to image an object, X-rays are focused using a lens. The resolution of one such image would be limited according to the following formula:

$$d > \frac{0.61\lambda}{NA} \tag{2.6}$$

where d is the resolution by a perfect lens limited by diffraction, λ is the wavelength of x-rays, and NA is the numerical aperture of the lens [107]. Looking at equation 2.6 it is clear that in order to improve the resolution one can either shorten the wavelength of the X-rays or increase the numerical aperture of the lens. In coherent diffractive imaging, one does not use a lens and thus the resolution of any generated image would not be limited by the numerical aperture of the lens. Instead limiting factors to the resolution would, amongst other things, be connected to quality of the sample to be imaged, radiation damage to the sample, and X-ray flux. While the prospect of coherent diffractive imaging is exciting, it comes with a number of problems. One such issue is that when using short wavelength X-rays with a high flux the chance of damaging proteins or other molecules of interest increases [108, 109]. In 2000 Neutze et al. published a paper arguing that one could "outrun" damage induced by radiation by using very short exposure times [110]. Doing so would allow retrieval of diffraction patterns from a biomolecule before it has had time to break down, thus circumventing the problem of radiation-induced damage by applying the "diffraction before destruction" approach . Other issues when using coherent diffractive imaging remain, however. When reconstructing an image one seeks to retrieve the wave function in the exit surface plane of a probed sample. This wave function can be expressed as:

$$\psi = Ae^{i\phi} \tag{2.7}$$

where A is the amplitude of the complex wave and ϕ is the phase. In coherent diffractive imaging, information about the phase is lost and is usually obtained by iterative phase retrieval algorithms. To demonstrate

an example of one such algorithm we define a function Ψ where $\Psi = \mathcal{F}(\psi)$ (the Fourier transform of ψ). The modulus of Ψ is then expressed as:

$$\Psi_{mod} = \sqrt{I}e^{i*arg(\Psi)} \tag{2.8}$$

where I is the measured intensity as expressed in equation 2.5 and the arg function extracts a phase angle from a complex expression. A simple example of a phase retrieval algorithm would then be:

$$\psi_{n+1} = \mathcal{F}^{-1}(\sqrt{I}e^{i*arg(\Psi_n)}) \tag{2.9}$$

where n increases until the function converges. [111] These phase retrieval algorithms paired with "diffraction before destruction" makes coherent diffractive imaging a potentially powerful tool for imaging biomolecules.

2.2.3 Time-Resolved X-ray Solution Scattering

While knowing the structure of a specific protein is a good start, more information is often needed in order to fully understand the movements and changes undertaken by said protein during its mechanism of action. One method used to obtain this information is Time Resolved X-ray Solution Scattering (TR-XSS) [112]. In TR-XSS, one takes snapshots of a protein in motion using short X-ray pulses and temporally arrange these snapshots, creating a "*movie*" of sorts, showing the movements of the protein. In order to sort the snapshots in time, one need to be able to activate a protein (activate in this case referring to the induction of a proteins functional movement) at a well defined time-point and then probe the protein at a time delay after activation. One way to activate a protein is via photoactivation where a flash of laser light hits a flowing protein containing a sample in solution [113,114]. The laser flash, set to a wavelength optimized to activate the protein, marks the start the protein movement. The protein is then hit by a flash of X-rays at a well defined time-point after the activation, capturing the diffraction pattern of the protein at that time point. The collected data is usually presented as difference-curves, comparing the radially integrated diffraction pattern from an unperturbed protein to that of a activated protein at time t_n. An illustration exemplifying this can be seen in figure 2.4.

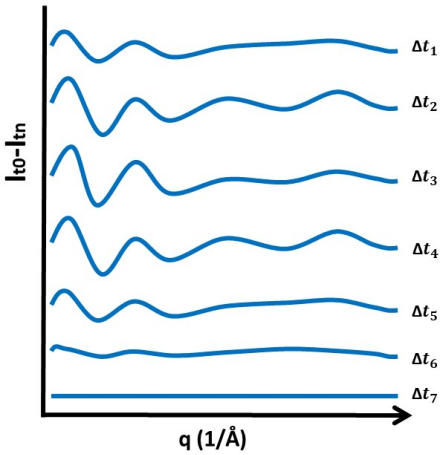

Figure 2.4: An illustration of what data obtained from a TR-XSS-experiment could look like. Small differences can be seen when comparing an unperturbed protein to the same protein at time t_1 after activation. This difference takes on different forms as other time-points are probed (t_1 - t_6). In this example the protein returns to its original state ate time t_7, showing no difference from the unperturbed protein.

These differences in radially integrated intensity are then usually compared to simulations of protein solution diffraction in different states in order to finally obtain a dynamic structure of the protein [115–118]. In **paper 3** we use utilize microwave fields in a TR-XSS-study to investigate the effects of electric fields on polymerized microtubules in solution.

2.3 Device Design

Most of the papers presented in this thesis made use of different devices designed to deliver an electric field onto a sample of protein. Two main designs were used, one delivering a lower electric field with a higher frequency, and one delivering a higher electric field with a lower frequency. The latter was designed in-house and the former was designed and built by Christer Stoij at Clear Sky Technology.

2.3.1 Gigahertz Waveguide

The high frequency design, here referred to as the gigahertz waveguide, is a dedicated capillary holder that has been developed such that a quartz capillary is positioned between a thin copper waveguide (50 μm) and a steel ground. Between the copper waveguide and the ground is a 1 mm deep slit designed to fit a 1 mm capillary. The device can be easily connected to a voltage source and has a 50 Ω load at the end of the waveguide. Illustrations of the gigahertz waveguide can be seen in figure 2.5.

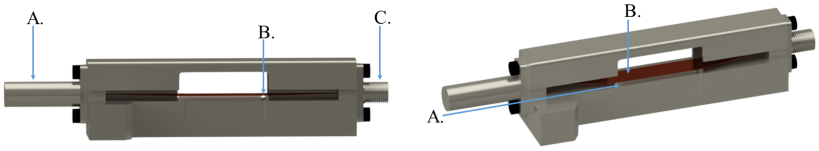

(a) A direct view of the gigahertz waveguide.

(b) A slightly tilted view of the gigahertz waveguide.

Figure 2.5: The gigahertz waveguide device. (a) A: 50 Ω load. B: Hole made at point where highest electric field strength was expected. Hole was made to make probing of sample using light scattering easier. C: Voltage source connector. (b) A: Slit for capillary. B: Copper waveguide.

The voltage source consisted of a commercially available signal generator (MG3694C Signal Generator 40 GHz, Anritsu), capable of generating alternating electrical fields (sinusoidal AC, 9.9 V peak to peak) ranging from kHz to GHz.

2.3.2 High Voltage Device

Part of the scope of this PhD-project was to design a device that could deliver a high voltage electric field over a sample of microtubules in solution. The device needed to be compatible with a previously procured custom-made voltage source capable of delivering a peak-to-peak voltage of 800 V at a frequency of 240 kHz. This device went through many fundamentally different design iterations but only the development of the final product design will be showcased in this chapter. The iterative process

of creating the device was done in collaboration with the department of Electric Power Engineering at Chalmers University of Technology. Design work was done using Autodesk AutoCAD©. Designed concepts requiring high detail were produced using 3D printing in a MAX/MAX UV, Asiga technologies printer using plastic resin (Asiga PlasGRAY V2). Designs too big for the Asiga printer were printed with a FELIX Pro 3 Touch from FELIXprinters using PLA filaments. A basic requirement for the device was that it be able to deliver a reproducible electrical field to a sample. In order to achieve this it was deemed essential to use electrodes of an easily determined shape. Spherical brass electrodes, 10 mm in diameter, were thus purchased from Guangzhou Decok Steel Ball Co., Ltd. and a plastic housing for these electrodes was designed. The design of the electrode housing unit also included a 0.6 mm diameter hole made to fit a quartz capillary containing microtubule samples. Grooves for fibre optic cables, capable of probing the point on the capillary where the highest electric field strength was expected, were also added to the design. The electrode housing unit can be seen illustrated below (figure 2.6).

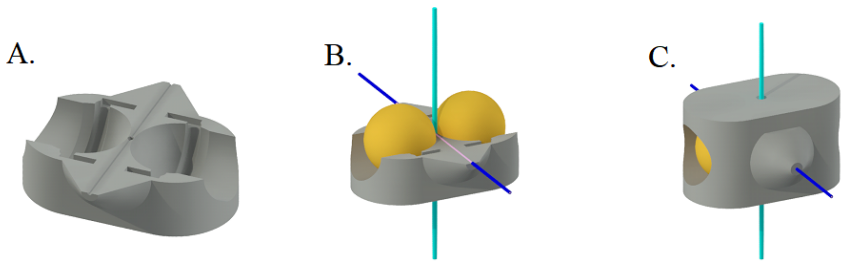

Figure 2.6: Design of the electrode housing. A: Lower half of housing with space for the spherical electrodes. B: Same lower half of housing with spherical electrodes (gold colored), quartz capillary (turquoise colored), and optical fibre (blue and pink), visualized. C: Both halves of the housing placed together with components. Rectangular grooves were added on lower part of housing made to fit rectangular protrusions on the upper part to allow for precise alignment of the two halves.

The housing at this stage was difficult to use practically, as it did not

have any place to add supports needed for it to remain steady during measurements. Also, since tweaking of the internal components of the housing (capillary, optic fibre, and electrodes) was sometimes required, something that held the housing together with something other than glue was deemed necessary. To solve these issues, a holder was designed that allowed for attachment onto an optomech post. The holder was made to contain supports for the quartz capillary, which otherwise tended to break when moving the device. Lastly, Safe High Voltage (SHV) connectors had to be secured in contact with the spheres. Cylindrical holes were thus added to the holders which could be threaded to fit the SHV-connectors. These designs are illustrated in figure 2.7 and figure 2.8.

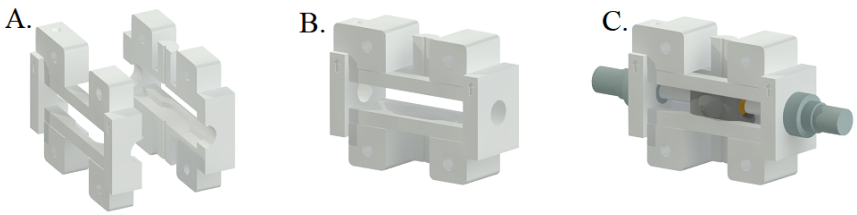

Figure 2.7: Holder designed for the electrode housing unit. A: The two separate parts of the holders. B: The holders as seen pushed together. C: Holders pushed together with internal components in place. In the center can be seen the electrode housing unit. To the left and right SHV-connectors are shown.

A more detailed illustration of the housing holder with all components can be seen in figure 2.8.

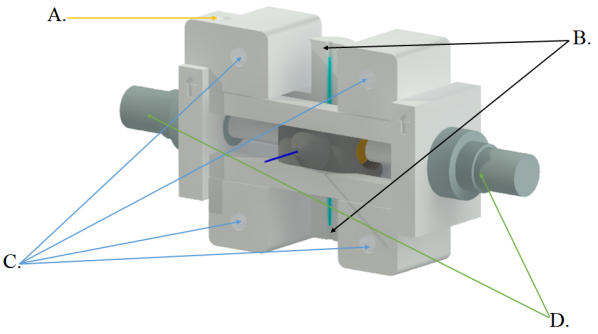

Figure 2.8: Holder for electrode housing unit in greater detail. A: Attachment point for optomech post. B: Supports for quartz capillary. C: Holes for screws, together with bolts allowing the holder to be tightly secured. D: SHV-connectors, connecting the device to the voltage source.

The device, once connected to the power source, formed a simple circuit illustrated in figure 2.9. The circuit consisted of a AC-voltage source with a 50 Ω load. The device, with its two separated electrodes and an electric field in between, acted as a capacitor where one of the spherical electrodes was always connected to ground.

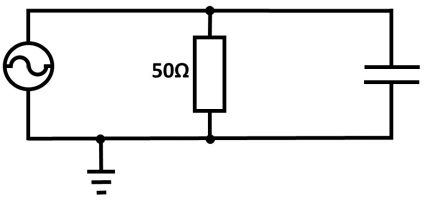

Figure 2.9: A simple circuit diagram illustrating the connected device and voltage source. Leftmost is the voltage source, giving out a sinusoidal AC-voltage. Middle is shown the 50 Ω load that helps reduce risk of a short-circuit as well as hinders reflections in the electrical signal. To the right is the device itself, illustrated as a capacitor. On the bottom is the ground.

The setup was tested at the department of Electric Power Engineering

at Chalmers University of Technology in order to ensure that no electrical discharges occurred during operation and that the circuit operated safely.

Chapter 3

Paper 1

In this paper titled "***No Observable Non-Thermal Effect of Microwave Radiation On The Growth Of Microtubules***" we investigate the effects of electric fields on the polymerization of microtubules subjected to microwave radiation using light scattering at 365 nm. After analysing the data it was concluded that no non-thermal effects can be observed.

3.1 Experimental Design

A waveguide device, mentioned in section 2.3, was used to measure the turbidity of polymerizing microtubules under GHz electric fields. The waveguide fits a 1 mm diameter quartz capillary within which the polymerizing tubulin sample was held during data collection. Data were collected by illuminating the polymerizing sample with 365 nm light from an LED. The change in optical density was monitored using a spectrophotometer. It was important to control the ambient heat of the sample so that the effect from heat on polymerization could be compared with the effect from the applied electric fields. For this purpose a temperature-controlled box was constructed. The walls of the box were made of acrylic glass and the temperature was controlled via hot air flowing into the enclosed space from a hot air gun. The temperature inside was monitored by thermometers. An IR-camera was also installed within the box to monitor the heat within the capillary situated in the waveguide. Images and illustrations of setup and waveguide can be seen in figure 3.1.

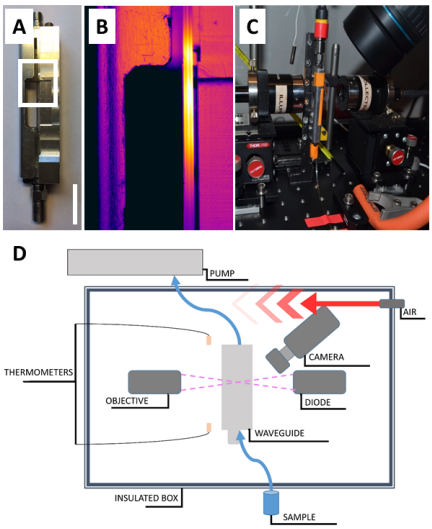

Figure 3.1: Depictions of the experimental setup. A: The waveguide seen from the side. B: Enlarged view of the waveguide with IR-camera. Warmer areas are shown in brighter colors. The image shows that the waveguide delivered the microwaves in a non-uniform manner along the capillary. Polymerization of microtubules was monitored at the brightest point as this was considered the point where the electric field was most intense. C: picture of the setup within the temperature-controlled box. D: Illustration of the setup. Sample was transferred from ice into the box where it reached a higher temperature and started polymerizing. The process was measured via absorption of 365 nm light focused by a diode and captured with an objective.

3.2 Sample Preparation

Tubulin was taken from a -80°C freezer, thawed on ice and diluted to a final concentration of 10 mg/ml by addition of GTP (final concentration 2mM), glycerol (final amount 10% by volume), and general tubulin buffer. The mixed sample was put on ice, and a syringe pump sucked the sample to the point of measurement as described in figure 3.1.

3.3 Data Collection

Samples were exposed to microwaves of varying frequencies and strength, ranging between 3.5 to 29 GHz and 15 to 23 dBm. Control samples were also recorded where the electric field was turned off. Measurements were additionally repeated without any electric field present but where the heat-profile caused by the microwaves was mimicked. This was done using either a focused IR-laser or the hot-air stream. For each measurement, the temperature of the sample at the point of measurement was recorded using the IR-camera. Each data-point was repeated on average 24 times.

3.4 Data Analysis and Results

Resulting data came in the form of time-dependent curves showcasing the change in OD as microtubule polymerization progressed. The variation within each data-point was quite high, which could be attributed to a number of factors. The samples introduced into the waveguide were quite small (about 5 μL), and since microtubule nucleation and growth are stochastic processes, internal variation is reasonable. This, and the fact that microtubule polymerization is sensitive to many different parameters [49] which could differ between runs, are likely reasons for the observed variation. This variation was taken into account when comparing different data-points.

When comparing the different polymerization curves, we looked at three different parameters: final OD of the sigmoidal curves, the time it takes a curve to reach 10% of its plateau-value (t_{10}), and the b-value. The b-value is derived from a power law that can be used to approximate microtubule growth in its initial growth phase [49]:

$$OD(t) = A\left(\frac{t}{t_u}\right)^b \tag{3.1}$$

where A is a constant, t_u is an arbitrary time unit introduced to make equation 3.1 dimensionless, and b is the power law exponent, or b-value. By taking the natural logarithm of equation 3.1 one gets:

$$ln\big(OD(t)\big) = ln(A) + b\big(ln(t) - ln(t_u)\big) \tag{3.2}$$

which shows that one can obtain the b-value by plotting $ln\big(OD(t)\big)$ vs. $ln(t)$ and extracting the slope of the line. The process of extracting t_{10} and b-values from a polymerization curve is illustrated in figure 3.2A,B.
In order to separate thermal from non-thermal effects when analyzing the results, "time stretching" was introduced. The assumption was that if the different phases in microtubule polymerization- nucleation, elongation, and saturation- co-vary with temperature, then the shape of a sigmoidal curve will be the same for varying temperatures. This stretching was made by matching the t_{50}-values (the time when polymerization reached 50% of its maximum value) of the different curves in time. Examples of this sort of time-stretching can be seen in figure 3.2C plotted together with standard error. Standard error was calculated using the equation $\sigma/\sqrt{N-1}$ where σ is the standard deviation and N is the number of repeats of one data point.

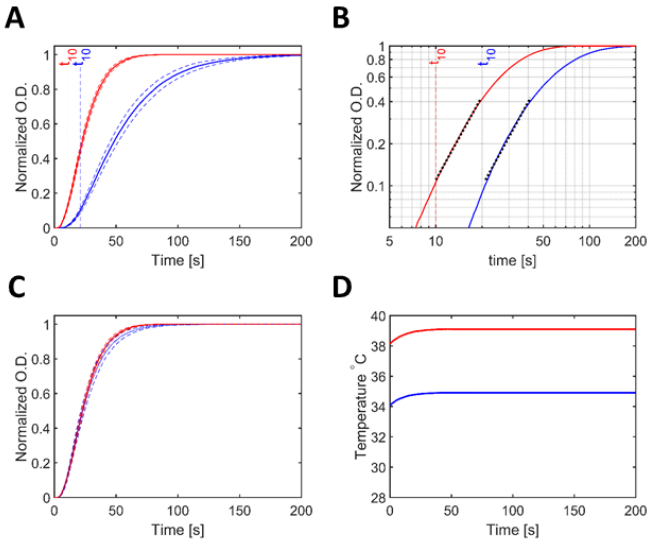

Figure 3.2: Normalized (max OD = 1) polymerization curves produced for two different temperatures 34.9°C (blue line) and 39.1°C (red line) with no external electric field applied. A: t_{10}-values were obtained by extracting the time at which the OD reaches 10% of its maximum value, with standard error for curves shown in dashed lines. B: The b-value was obtained by extracting the slope of the line in a log-log plot. C: Stretching the blue line onto the red line shows that even though the lines were polymerized under different temperatures, the final shape of the polymerization curves are similar. Standard errors for curves are shown in dashed lines D: The temperature recorded at the point of measurement for both samples.

If an applied electric field were to change the behaviour of any of the microtubule phases, then the shape of this curve would be expected to differ from a curve obtained under similar conditions, but with no field applied. An example of this can be seen in figure 3.3.

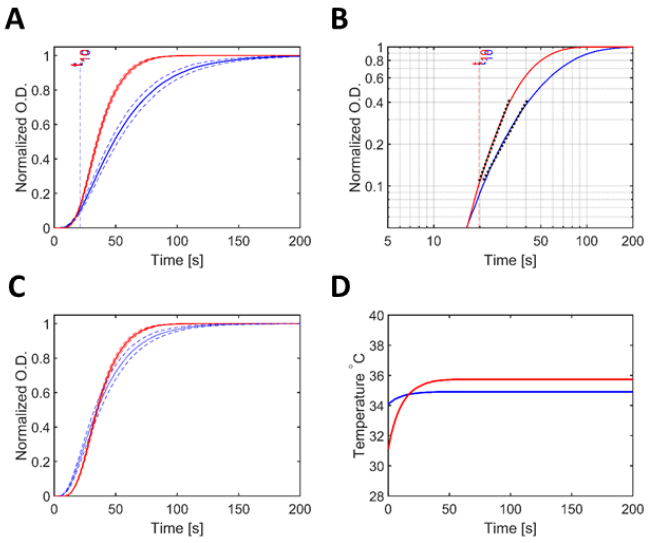

Figure 3.3: Normalized (max OD = 1) polymerization curves produced for two different conditions, 34.9°C with no external electric field applied (blue line), and 34.9°C with a 23 dBm, 20 GHz electric field applied (red line). A: The two normalized curves. t_{10}-values are close to overlapping, with standard error for curves shown in dashed lines. B: The log-log plot of the curves yields lines of different slope, b-value differ. C: Curves after applied time-stretch. The curves can be seen to be of different shape, with standard error for curves shown in dashed lines. D: The temperature of the point of measurement remains fairly close for the most part.

As can be seen in figure 3.3C, the resulting curves after stretching have significantly different shapes, indicating that there might be a non-thermal effect on the polymerization as a result of the applied electric field. However, looking at figure 3.3D, it is clear that while the final temperatures at the measurement point are similar, the initial temperatures differ. This difference in thermal history arises from efforts to ensure that the temperature of the polymerizing samples under both conditions is the same at the point of measurement. Since it is well known that microwaves induce heating, the ambient temperature of the box was lowered during runs when the electric fields was applied. Thus, for those runs the

samples traveled through a colder environment prior to the point of measurement, potentially affecting polymerization. In order to control for this phenomenon, the point of measurement was heated by an IR-laser in a way that would mimic the heating effect from the microwaves. The result of this IR-laser heating is represented in figure 3.4.

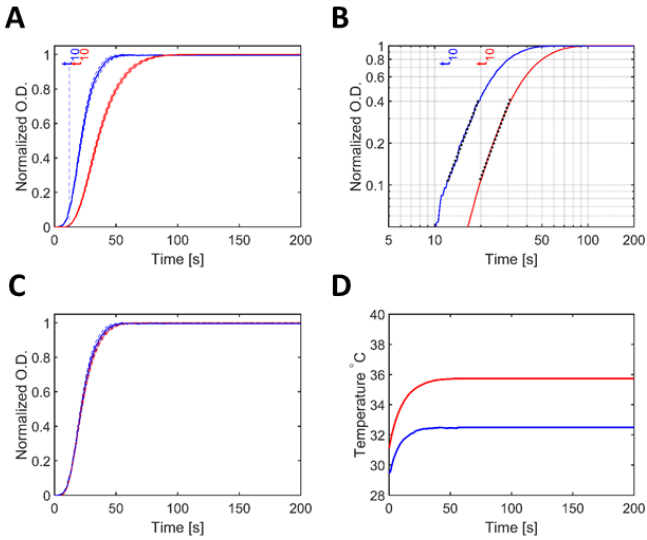

Figure 3.4: Normalized (max OD = 1) polymerization curves produced for two different conditions: 31.9°C heated with IR-laser with no external electric field applied (blue line), and 34.9°C with a 23 dBm, 20 GHz electric field applied (red line). A: The two normalized curves with t_{10}-values. Standard error for curves shown in dashed lines. B: The log-log plot of the curves yields lines of similar slope. C: Curves after applied time-stretch. The curves are seen to be very similar, with standard error for curves shown in dashed lines. D: The temperature of the point of measurement.

As can be seen in figure 3.4C, the shapes of the time-stretched curves are very similar, indicating that the thermal history was responsible for the effects seen in figure 3.3. In order to ensure that the results observed when heating with the IR-laser were not due to some effect caused by interaction of the polarized IR-laser light with the microtubules in an

orientation-dependent way, an additional control was made. In this control a stream of hot air flowed over the point of measurement, mimicking the heat profile induced by the microwaves and the IR-laser. Results from these experiments are represented in figure 3.5.

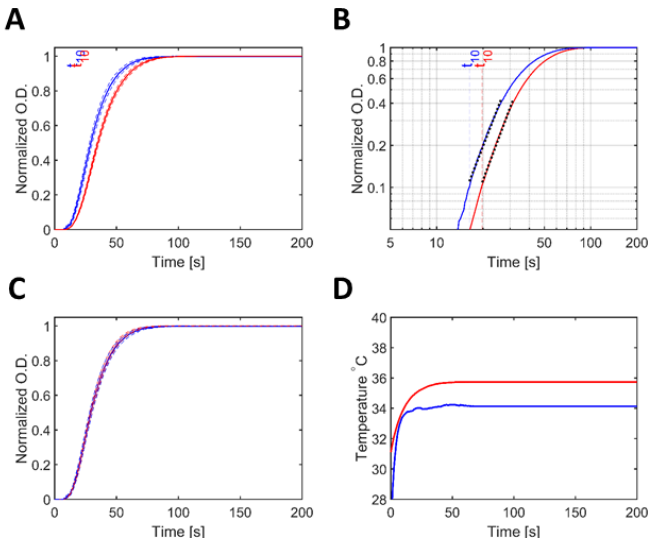

Figure 3.5: Normalized (max OD = 1) polymerization curves produced for two different conditions: 34.1°C heated with air-stream with no external electric field applied (blue line), and 34.9°C with a 23 dBm, 20 GHz electric field applied (red line). A: The two normalized curves with t_{10}-values. Standard error for curves shown in dashed lines. B: The log-log plot of the curves yields lines of similar slope. C: Curves after applied time-stretch. The curves can be seen to be very similar, with standard error for curves shown in dashed lines. D: The temperature of the point of measurement.

As can be seen in figure 3.5C, the shapes of the time-stretched curves are again similar. The theory that the differences seen in figure 3.2 are due to the thermal history of the sample seems likely.

The data shown in figures 3.2-3.5 were chosen as they are representative of results obtained throughout the study. Many other combinations

of temperatures, fields strengths, and frequencies were used, all pointing to the same overall result.

3.5 Final Comments and Conclusion

During recent years there has been growing public concern regarding radiation from microwave fields, igniting debate and controversy [18, 22]. Specific worries have been voiced regarding the effect of mobile phones, as well as expanding 5G-networks [16, 17]. The lack of non-thermal effects seen in our study adds to the argument that neither mobile phones nor 5G towers should have any negative effect on biological systems. It should, however, be noted that the possibility of negative effects from any type of commonly occurring high frequency fields can not be excluded, and that more studies should be conducted.

In an earlier iteration of this study performed by our group it was concluded that microwave fields *did* have a non-thermal effect on the polymerization of microtubules [119]. This conclusion was reached because consideration had not been given to the effect thermal history would have on the sample, and all data collected was of the type seen in figure 3.3. When control measurements were performed using the IR-laser it was expected to support the conclusions made. However, this was not the case. After significant redesign to the experimental setup, more control measurements were made, all pointing to the results shown in this paper.

The polymerization of microtubules is a complicated process with many variables and components which can all be affected by external factors in different ways [49, 51]. The complexity of microtubule assembly, together with the journey of this particular investigation, helps to highlight the importance of carefully planned studies. The absence of rigid experimental design is a reoccurring criticism of many other studies aiming to investigate the effects of high frequency fields on microtubules and other complex biological systems.

Chapter 4

Paper 2

In this paper titled "***Influence of Oscillating Electric Fields on the Growth of Microtubules***" we investigate effects of electric fields on the polymerization of microtubules subjected to high voltage kHz-fields using light scattering at 365 nm. Four frequencies ranging from 100-240 kHz were tested. Initial results indicate that the polymerization of microtubules are affected by these kHz fields to a small degree.

4.1 Experimental Design

In order to deliver a high voltage field in the kHz domain, a device capable of doing so was designed as described in section 2.3.2. The device was lowered into a 12 L container of transformer oil, which served as a means to hinder any potential electric discharges. The temperature of the oil was controlled using a thermostat and was kept at 37°C. The thermostat caused the oil in the container to flow, which disturbed the optic fibres used for probing tubulin polymerization, causing very noisy and poor readings of the polymerization. To counteract this effect, stabilizers for the optic fibres were designed and added to the electrode housing unit. The housing unit, as well as a schematic of the setup can be seen in figure 4.1

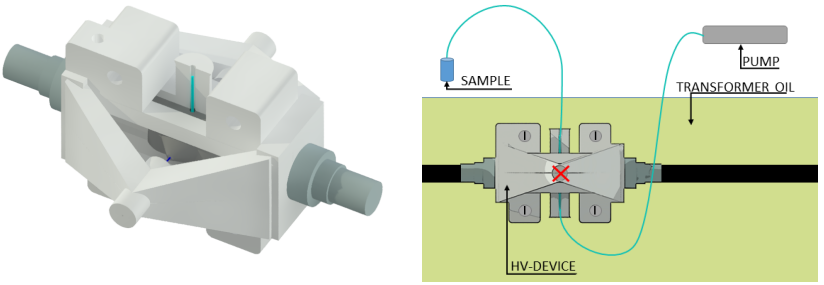

(a) High voltage device.

(b) Experimental setup.

Figure 4.1: Illustration of the design of the high voltage device with housing, as well as the overall experimental setup. (a) shows high voltage device and housing unit together with fibre optic stabilizers. (b) shows the entire experimental setup submerged in oil. Probing position of microtubule polymerization marked with red cross.

4.2 Sample Preparation

Tubulin was taken from -80°C freezer, thawed on ice and diluted to a final concentration of 10 mg/ml by addition of GTP (final concentration 2mM), glycerol (final amount 10% by volume), and general tubulin buffer. The mixed sample was put on ice and a syringe pump sucked the sample from ice to the point of measurement marked by red cross in figure 4.1.

4.3 Data Collection

The sample of tubulin was exposed to an alternating electric field. The voltage on the voltage bearing sphere measured 800V peak-to-peak. Tubulin was allowed to polymerize under the effect of four frequencies, 100 kHz, 147 kHz, 193 kHz, and 240 kHz. Control measurements were also carried out where tubulin was allowed to polymerize without the influence of an external electric field.

In order not to introduce a bias in the obtained data as an effect of the order of the conducted experiments, specific frequencies (or lack thereof)

were applied in a randomized fashion for the generation of each obtained polymerization curve. Each data-point was repeated on average 34 times.

4.4 Data Analysis and Results

As in **paper 1**, the variation within each datapoint was quite high. In order to better be able to compare the shapes of the sigmoidal polymerization curves for the different datapoints, all curves were normalized and stretched in time to the same t_{50}-value. An example of this stretching in time can be seen in figure 4.2. When comparing different polymerization curves it was decided to look at three different parameters. These parameters being the time it takes the polymerization to reach 80% of its final plateau-value, the t_{80}-value, as well as the t_{10}-value and the b-value. The t_{10}- and b-values were obtained as described in section 3.4.

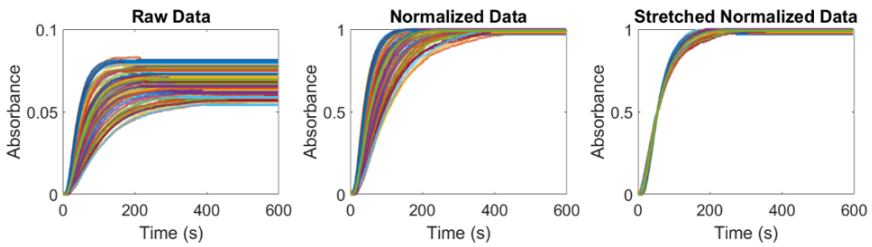

Figure 4.2: Example of data normalization and stretching. Left shows batches within the same data point with batch-to-batch variation being very large. Middle show the same data after normalizing. Right show the data after normalizing and stretching.

Figure 4.2 illustrate that stretching in time results in a more comparable dataset. After stretching, in order to further clean the data, all curves were normalized and strong outliers were removed. The time-stretched and normalized curves can be seen for each dataset in figure 4.3.

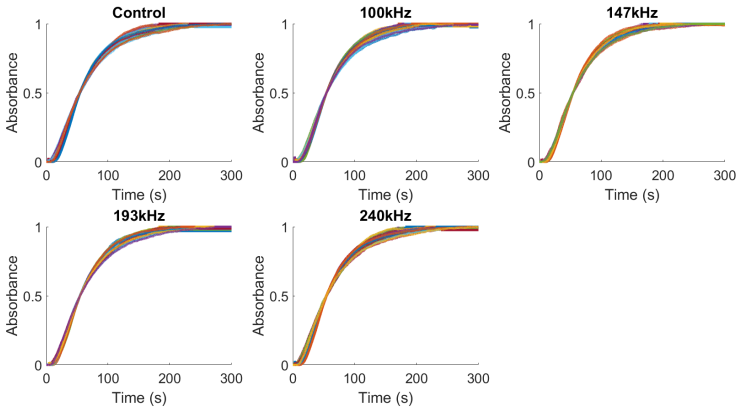

Figure 4.3: Time-stretched and normalized polymerization curves for each dataset. Since every datapoint was stretched to a common t_{50}-value, all curves intersect at this point.

Every data-point within a dataset was averaged and the resulting averages were overlaid and plotted together with standard error defined as $\sigma/\sqrt{N-1}$ where σ is the standard deviation and N is the number of repeats for a data-point. These curves, as well as zoomed-in comparisons between the different applied fields and the control, can be seen in figure 4.4.

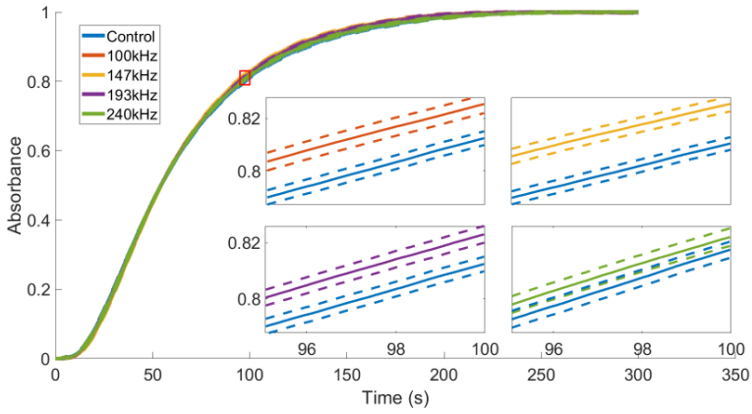

Figure 4.4: Overlaid averages of each time-stretched and normalized datapoint curves with included standard errors (dashed lines). Curves obtained under different applied external electrical fields are shown compared to the control value around t_{80} (area marked by red box).

The averaged curves seen in figure 4.4 show that there might indeed be a difference in shape between the curves around the t_{80}-timepoint. To further investigate this difference t_{10}-, t_{80}-, and b-values were extracted and plotted for each time-stretched and normalized curve before averaging. These values for each subset can be seen in figure 4.5.

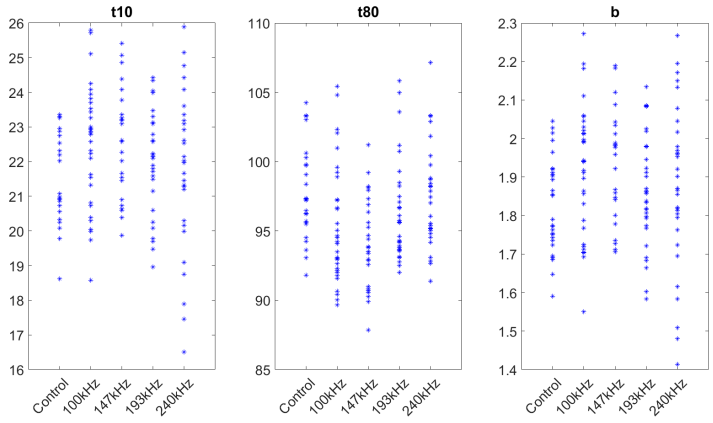

Figure 4.5: Graphs showing the t_{10}-, t_{80}-, and b-values for each curve making up the different subsets.

Looking at figure 4.5 it can certainly be said that there is still a spread within each subset even after time-stretching. The values for the different parameters can also be seen to overlap on many points. However, one can spot some trends, most clearly seen when looking at t_{80}- and b-values for the 100 kHz and 147 kHz subsets when compared to the control. Thus, two-component t-tests were performed, comparing parameters for each subset of polymerization curves obtained under the applied electric fields. The results of these t-tests can be seen in table 4.1.

Table 4.1: The exact values for the p-values obtained during the initial t-test.

p-values	t_{10}	t_{80}	b
100 kHz	0.0376	0.0140	0.0201
147 kHz	0.0268	9.79×10^{-5}	0.0151
193 kHz	0.3437	0.0609	0.3279
240 kHz	0.5846	0.3756	0.3098

The p-values listed in table 4.1 do not show very low values. Usually for experiments such as these where the spread within subsets is so big we look for p-values below 10^{-4} when comparing between subsets, which is usually regarded as stringent. Apart from the t_{80}-values seen when

comparing 147 kHz to control, our condition for a significant difference is not met.

In order to make sure that no sub-populations within our subsets skewed our results we decided to perform a comparison using a set consisting of randomly selected half of the data versus the other half. This random sampling comparison was first done internally, comparing a random half of a specific subset with the remaining half in order to illustrate what would statistically be expected when comparing a subset to itself. After this internal comparison, further comparisons were made between subsets. This random sampling method is illustrated in figure 4.6.

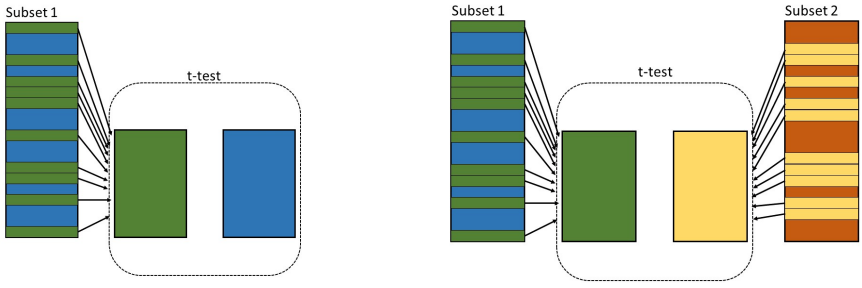

(a) Internal comparison using random sampling.

(b) Comparison between subsets using random sampling.

Figure 4.6: Illustration of the random sampling comparison used. (a) illustrates how samples were compared internally. One sub-population was randomly selected from a subset of data. A two-component t-test was then performed between the two halves of the subset. (b) illustrates the randomized comparison between two subsets. Half of each subset was randomly selected and a two-component t-test were performed between the selected halves.

The random selection and t-test, illustrated in figure 4.6, were performed 1000 times for each comparison. The amount of t-tests that indicated a significant difference (5% cutoff) were added up for the different comparisons. The results for the 1000 internal comparisons can be seen in figure 4.7.

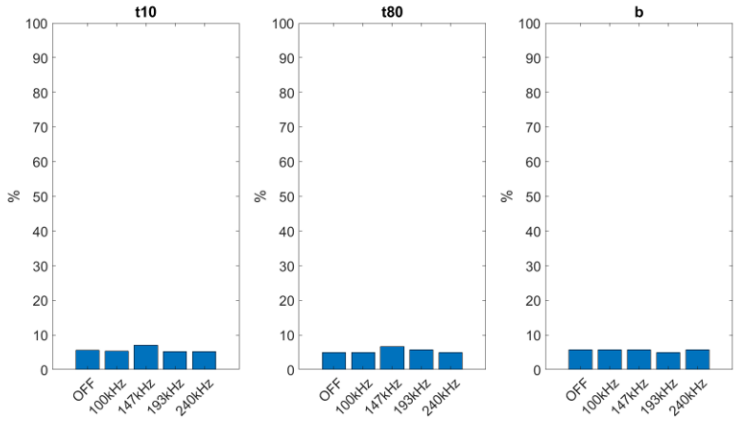

Figure 4.7: Randomized internal comparison. Random internal comparisons were performed 1000 times using two-components t-tests. The percentage of times the t-test resulted in a significant difference between the two randomly selected sub-populations are listed for each data subset.

The highest occurrence of significant difference between randomly selected sub-populations is found when comparing the control with itself, just below about 8% for t_{10}- and b-values. Other internal comparisons remain below 5%, which is the expected value for internal comparisons of populations with a normal distribution around the same mean. Next comparisons were made between the subsets consisting of polymerization curves subjected to electric field versus the control subset. These comparisons are shown in figure 4.8.

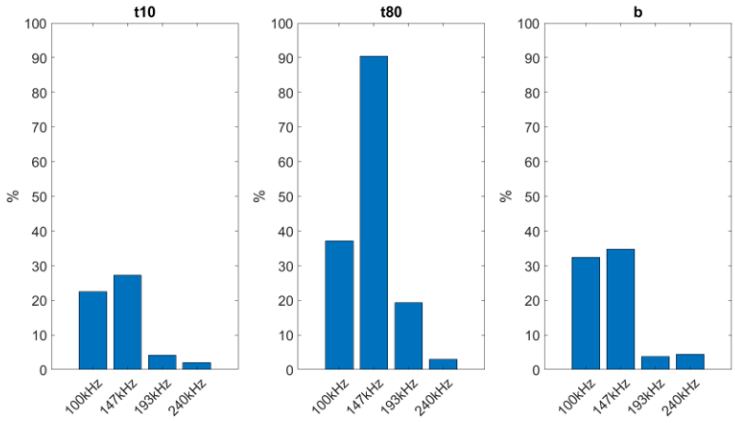

Figure 4.8: Randomized comparison between subsets from curves obtain under influence of electric fields and the control subset. Random comparisons were performed 1000 times using two-components t-tests. The percentage of times the t-test resulted in a significant difference between the randomly selected sub-populations are listed for each data subset versus the randomized sub-population of the control subset.

As can be seen in figure 4.8, the randomized comparison between subsets 193 kHz and 240 kHz versus the control resulted in relevant differences about as often as for the internal comparisons seen in figure 4.7. One slight exception occurring when comparing t_{80}-values of 193 kHz to the control. Both 100 kHz and 147 kHz versus the control show significant difference more often than the internal comparisons, but still for less than 50% of the times the t-tests were performed. An exception to this trend is seen when comparing t_{80}-values of 147 kHz to the control, with statistically relevant occurrences close to 90%. This data show that the effect of HV-fields in the TTF range of frequencies does not seem to significantly affect microtubule polymerization in solution with a possible exception for frequencies around 147 kHz and perhaps 100 kHz as well.

4.5 Final Comments and Conclusion

The study presented here has shown only subtle effects when subjecting polymerizing microtubules to high voltage electric fields in the TTF range of frequencies. The 147 kHz fields seem to stand out when comparing t_{80}-values to the control. Some differences can be seen for other parameters and other frequencies as well, but with our stringent $p \leq 10^{-4}$ condition only the aforementioned occurrence will be discussed in depth.
Looking at figure 4.5, the time when the polymerization reached 80% of its plateau-value seems to arrive sooner than for the control. Previous theories regarding the mechanism of TTFs efficiency in treating a range of tumours, theorize that the main part of the effect of oscillating electric fields on dividing cancer cells likely stem from the morphology of said cells [25, 26]. Furthermore, when using TTFs in cancer treatment, different cancer types are best treated using different frequencies in the TTF-range, this frequency dependence is also contributed to cancer cell morphology in the target tissue [26]. The results presented in this thesis where the intermediary frequency of 147 kHz appear to induce perturbations in the microtubule polymerization when other applied frequencies do not, indicate a frequency dependency on the molecular level since the morphology of the sample remains the same throughout the experiments.

As previously mentioned in this thesis, microtubule polymerization is sensitive to an array of parameters [49]. As such, a high variation between datapoints obtained under seemingly identical conditions is common and comparison between subsets of data where polymerization conditions were made to differ can be difficult. While results presented in this study indicate that HV-fields with a frequency of 147 kHz can affect microtubule polymerization in an aqueous solution, a larger data set is required in order to, with higher certainty, see if this effect is present for other frequencies as well.

Chapter 5

Paper 3

In this paper titled "***Microwave Induced Orientation Perturbations Of Microtubules***" we investigate the effects of electric fields on polymerized microtubules subjected to electric fields in the microwave domain via X-ray probing. The study found that an applied microwave field gives a difference in diffraction signal corresponding to a change in microtubule orientation.

5.1 Experimental Design

Pre-polymerized microtubules were flown through a 1 mm capillary and exposed to microwave fields perpendicular to the direction of sample flow. These microwaves were delivered by a waveguide as described in section 2.3. Microwave exposure was performed in repeated cycles where one pattern consisted of 4 seconds of sample being exposed to 20 GHz microwaves, followed by 6 seconds without microwave exposure. Furthermore, the sample capillary was probed at different positions at varying distances from the capacitor plate on the waveguide where the voltage was applied. Probing position A was located 15 μm from the closest point to the capacitor plate where the plate itself did not significantly affect the detected X-ray diffraction. Position B was 50 μm away from position A, position C 150 μm away from position B, and position D 150 μm away from position C. An illustration of these positions can be seen in figure 5.1.

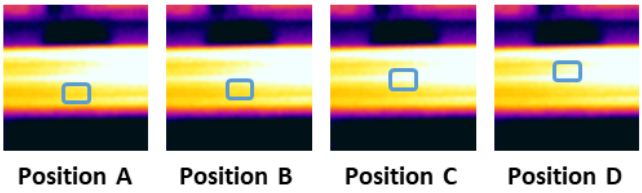

Figure 5.1: The different probing positions used in this study. Position A was located as close to the capacitor plate as was deemed reasonable. Position B was placed 50 μm away from A, C 150 μm away from B, and D 150 μm away from C.

5.2 Sample Preparation

Tubulin was taken from -80°C freezer, thawed on ice and diluted to a final concentration of 47 mg/ml by addition of GTP (final concentration 2mM), glycerol (final amount 10% by volume), and general tubulin buffer. The mixed sample was placed in a heat block at 37°C where it was allowed to polymerize. Polymerized sample was then pumped to the point of measurement using a syringe pump.

5.3 Data Collection

Throughout the experiment, sample was probed by a continuous X-ray beam and diffraction was registered by a detector at 25 Hz. A combination of WAXS and SAXS detectors were used in order to monitor both the induced heating of the sample from the microwaves (WAXS) and the perturbations of microtubules in the sample (SAXS). The time of each registered diffraction pattern was recorded in relation to the microwave application scheme, allowing for determination of temporal effects on the sample.

5.4 Results and Discussion

Diffraction from the flowing sample was collected at the different positions A-D. It became clear that the flow in the capillary resulted in

anisotropic scattering due to flow alignment of microtubules. Diffraction patterns showed more scattering in the equatorial plane than in the meridional plane. As such, the diffraction patterns were divided into two fields, equatorial (upper and lower quadrants of detector) and meridional (left end right quadrants of the detector). An example of a diffraction pattern, as well as the different fields can be seen in figure 5.2.

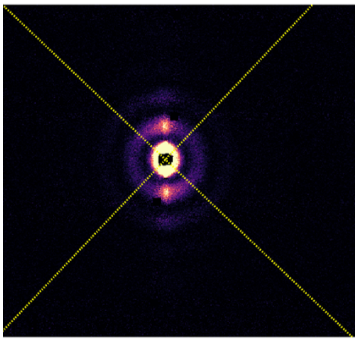

Figure 5.2: An example of a diffraction pattern from microtubules flowing in a capillary. Images were divided into equatorial and meridional planes as marked by yellow dashes. Higher intensities can be seen in equatorial planes as a result of flow alignment.

In order to compare degree of microtubule flow alignment at the different positions, a graph containing angular distributions of the recorded diffraction intensities were plotted. These angular distributions can be seen in figure 5.3.

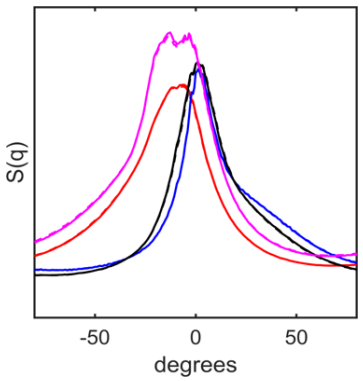

Figure 5.3: Angular distributions of detected intensities at the different probing positions. Distribution at position A, B, C, and D can be seen in corresponding colors.

Figure 5.3 show that the angular distribution becomes more narrow as one moves further from the capacitor plate, with position C and D giving similar results. This can likely be related to the expected flow profile in a capillary. Alignment in points further from the capillary walls will be less affected by flow effects expected close to a wall.
As previously mentioned, measurements were taken both when sample was exposed to microwaves and when samples were not exposed to microwaves, these measurements were referred to as "on" and "off" respectively. In order to investigate effects of electric fields diffraction intensities for "on"-measurements were subtracted from intensities for "off"-measurements for every position investigated. The resulting difference curves can be seen in figure 5.4.

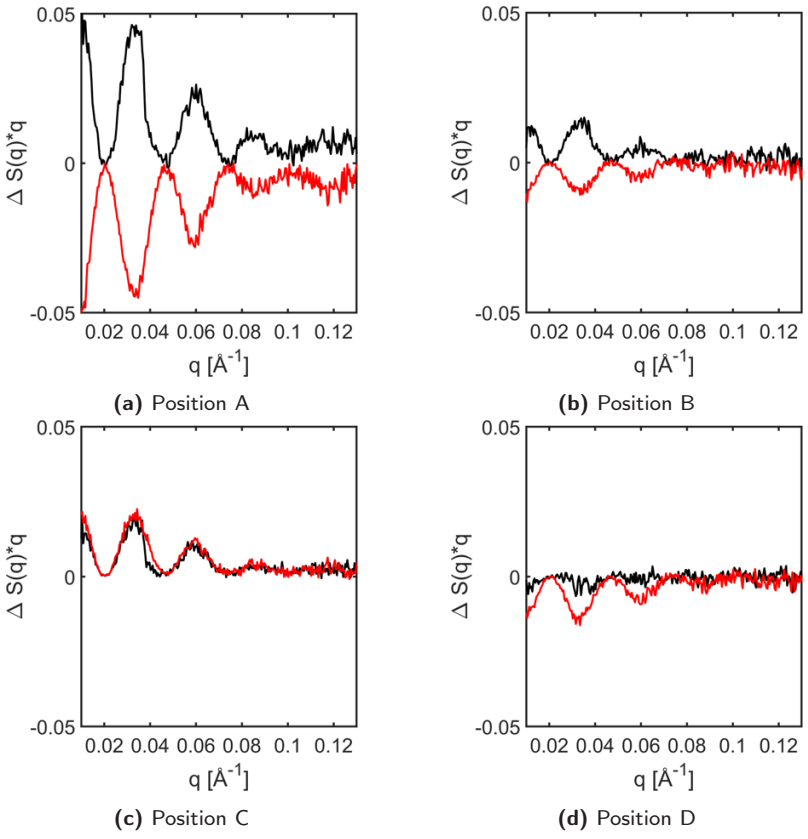

(a) Position A **(b)** Position B

(c) Position C **(d)** Position D

Figure 5.4: Difference curves for position A, B, C, and D shown in figure 5.4a, 5.4b, 5.4c, and 5.4d respectively. Black curves show difference in equatorial region. Red curves show difference in meridional region.

Graphs displayed in figures 5.4a and 5.4b imply that intensities increase in the equatorial plane and decrease in the meridional plane as a result of applied microwave fields. The effect seem to dissipate further from the capacitor plate, with a trend breaker seen for position C in figure 5.4c, and position D in figure 5.4d showing no discernable difference in the equatorial plane. This overall result seem to indicate that the electric fields increase flow alignment, which is counter intuitive since microtubules are expected to align parallel to the electric field direction.

To explain this counter intuitive phenomenon, remember that the differences shown in figure 5.4 were derived from a direct comparison between when microwaves were delivered to the sample and when they were not delivered to the sample. However, they did not give information regarding the change in intensity at more specific time-points throughout the microwave application scheme. In order investigate the change in intensity at these time-points new difference curves were obtained for position A, B, and C. These difference curves compared intensities obtained at a specific time t, taken after the start of the microwave cycle, with the average of the intensities obtained during the final 0.4 seconds of the cycle, denoted t_{ref}. The resulting expression for these differences being: $\Delta S(q,t) = S(q,t) - S(q,t_{ref})$, where $S(q,t)$ is the intensity.

All difference curves were put into a matrix M such that each column in the matrix consisted of a difference curve taken at time t, with the first column containing the difference curve for $t = 0$. Singular Value Decomposition (SVD) of this matrix gave $M = USV^T$, where U contained information relating to the overall shape of all difference curves and V contained information relating to how that shape changed over time. The main features of U and V were normalized with respect to V and plotted for position A, B, and C as in figure 5.5

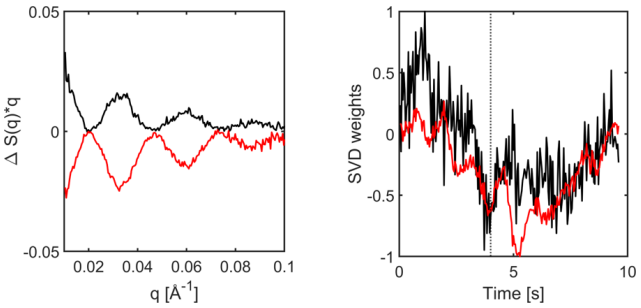

(a) Position A

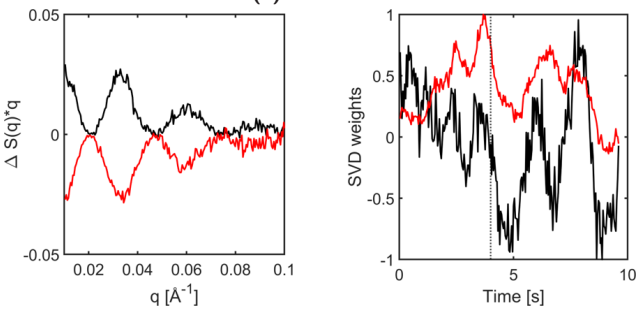

(b) Position B

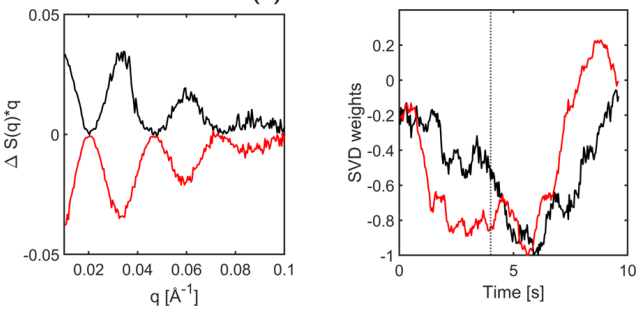

(c) Position C

Figure 5.5: Main features of U (left) and main features of V (right) for position A, B, and , C shown in figure 5.5a, 5.5b, and 5.5c respectively. Black curves show difference in equatorial region. Red curves show difference in meridional region. Delimiter between On and Off parts of the exposure cycle marked with a dashed line at 4 seconds.

As seen in the left part of figure 5.5, the overall shape of the difference

curves show a general tendency of intensities increasing in the equatorial plane and decreasing in the meridional plane. However, the right part of figure 5.5 show that during the time the electric fields are applied over the samples the weights go below 0 with the exception of the meridional weights in figure 5.5b. This overall trend indicate that during the first 4 seconds when the microwaves are turned on, the scattering increase in the meridional plane and decrease in the equatorial. Further inspecting the right hand side of figure 5.5 shows that even after the 4 second-mark the weights keep going down, this is likely due to the fact that a larger volume of sample is exposed to the electric field than is being probed by the X-rays. The microtubules previously affected by electric field will thus still be hit by X-rays even at a time-point when the microwaves are turned off. This delayed recovery of microtubule flow alignment seems likely to be the cause of results seen in figure 5.4. For this figure *all* off-measurements were subtracted from *all* on-measurements which, since most of the microtubules had yet to recover from the microwave effects, gave a counter-intuitive result.

5.5 Final Comments and Conclusion

Figure 5.5 help explain the counter-intuitive results seen in figure 5.4 and also indicates that applying microwave fields perpendicular to a flowing sample of microtubules causes a portion of the microtubules to orient themselves parallel to the electric field. This is consistent with theory that suggest alignment of microtubules when subjected to oscillating electric fields [67,120]. Any conformational changes within the microtubules, such as vibrations, as a result of perturbation by the electric field would in this study be difficult to detect. Any such signals would be drowned by the strong signal caused by microtubule alignment in both liquid flow and electric fields. This study can thus not be used to support the occurrence of vibrational effects in microtubules, which is in line with related studies where microtubules were subjected to electric fields in the THz domain [121].

Chapter 6

Paper 4

In this paper titled "***Coherent Diffractive Imaging Studies of Microtubules Using Megahertz Data-Collection***" we probe the structure of paclitaxel-stabilized microtubules in solution using X-ray scattering. In a previous paper by the group, stabilized microtubules in a small liquid jet were probed with an X-ray laser and the diffraction patterns were used to obtain the structure of a microtubule in solution [64]. While the study was successful it was determined that multiple microtubles were hit per X-ray pulse and that it should be possible to hit just a single microtubule by lowering protein concentration and decreasing the diameter of the liquid jet. In an attempt to do this we used a low concentration paclitaxel-stabilized microtubule solution and delivered these in a very thin liquid jet via a Gas Dynamic Virtual Nozzle (GDVN). Microtubules in the liquid jet diffracted at the EuXFEL outside of Hamburg. Reconstruction of a higher resolution microtubule structure was not achieved as of writing this thesis, but further data analysis is required.

6.1 Experimental Design

Microtubule samples were stabilized using paclitaxel and loaded into a GDVN. A GDVN uses a co-flowing gas, usually helium, in order to focus a stream of liquid into a very thin liquid jet [122]. An illustration of a GDVN can be seen in figure 6.1.

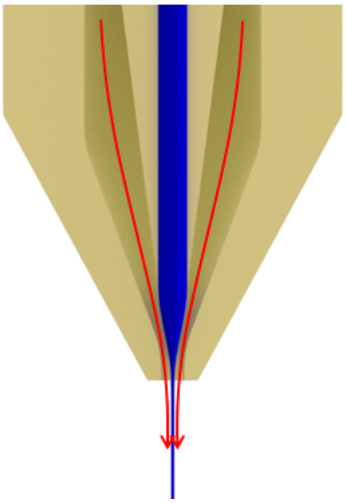

Figure 6.1: An illustration of a Gas Dynamic Virtual Nozzle. A stream of liquid (blue) flows in a capillary. At the end of the capillary a co-flowing gas (red) helps accelerate the liquid while keeping it stable, achieving a very thin jet.

In this study a GDVN was used to create a jet ranging between 4.3-6.4 μm in diameter, which resulted in liquid flow speeds of 37-42 m/s. The jet was probed by trains of pulses, where every train hit the jet at 10Hz. One train contained 352 pulses of X-ray radiation, which within the train were delivered at 1.1 MHz.
Initial diffraction patterns resulting from the smooth-flowing jet showed that scattering from the microtubules were shadowed by the signal from the liquid jet itself. In order to circumvent this problem the jet was made unstable and the X-ray pulses were allowed to blow up the jet. This caused microtubule diffraction patterns to become visible at random angles as pulses hit randomly oriented jet streaks and droplets. An example of an exploding unstable jet can be seen in figure 6.2.

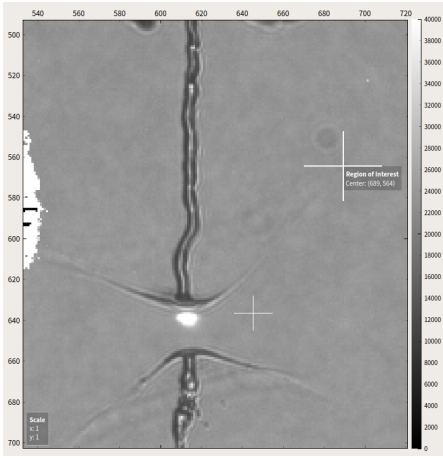

Figure 6.2: A snapshot of an unstable jet exploding as it is hit by X-rays pulses.

6.2 Sample Preparation

Tubulin was taken from -80°C freezer, thawed on ice and diluted to a final concentration of 5 mg/ml by addition of GTP (final concentration 2mM), glycerol, and general tubulin buffer. The mixed sample was placed in a heat block at 37°C where it was allowed to polymerize. Polymerized sample was then mixed with a paclitaxel solution to a final concentration of 2 mg/ml. The paclitaxel-microtubule solution was put into reservoirs that connected to the GDVN.

6.3 Results and Discussion

Initial data collection resulted in 268 million diffraction images, out of these 143 million were collected using the unstable-jet approach as described. In order to sift through these images in search for clear microtubule diffraction patterns, a rudimentary machine learning (ML) script was made. The script used a neural network, illustrated and explained in figure 6.3, trained to recognize radially integrated diffraction patterns corresponding to microtubule diffraction. The obtained diffraction patterns

were radially integrated and divided into 5 different groups: no detected diffraction (miss), diffraction from liquid jet, diffraction from microtubules, diffraction from small water droplets, and diffraction from unknown artefacts likely caused by the data collection scheme. These different groups were identified using the ML script which had as an output a binary vector of the general shape: [0 0 1 0 0], where an element with a value of 1 corresponded to the category of the identified image (the example given shows the output of an image identified as category 3, diffraction from microtubule). The ML-script was used in combination with a more conventional hit-finding script that sorted images based on position of intensity peaks. The hit finding scripts decreased the data to 31140 hits. Many of these hits contained unwanted artefacts and needed to be removed, resulting in about 10000 usable hits, corresponding to an effective hit rate of 0.009%. This is very low and could likely be improved by further work with the hit finding algorithms.

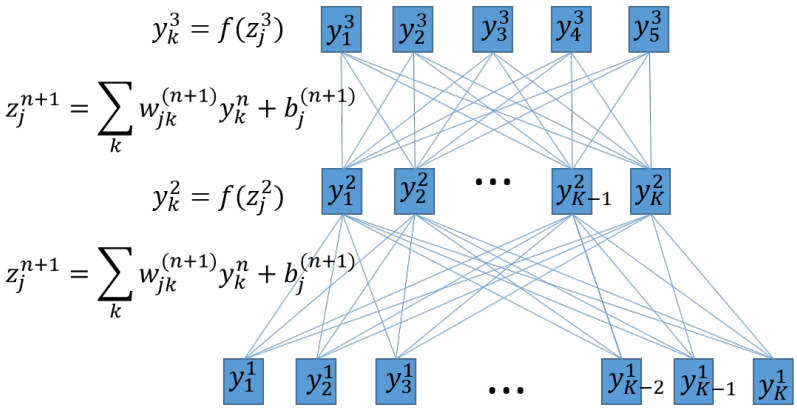

Figure 6.3: Illustration of the neural network used in the machine learning script. Vectors containing information from radially integrated diffraction data was fed into the first layer of neurons where the value of each neuron, y_k^1, correspond to one element in the vector. Each neuron on the first level were connected to each neuron in the second level via weights, w, represented as blue lines. Values for neurons in subsequent layers were obtained by applying an activation function on the sum of values of the neurons in the previous layer multiplied with their corresponding weights, this sum denoted as z, sometimes a flat bias value b was added as well. The weights and biases were designed to identify one of the five categories of diffraction, giving the final neurons a value corresponding to the type of diffraction image fed into the first layer of the network.

The found hits were rotated and averaged to form one diffraction pattern which can be seen in figure 6.4a. In the rotated and averaged pattern, however, there were no sign of any higher-order diffraction peaks. These higher-order peaks contain information about the internal structure of the microtubule and were expected to show up as horizontal lines parallel to the main central peaks. A 2D projection image was recovered from the diffraction pattern seen in figure 6.4a by use of a phase retrieval algorithm as well as using the inverse Fourier transform. This reconstruction, seen

in figure 6.4b, lack higher resolution, but still feature a tube-like appearance with a low electron concentration in the middle that increases as one moves outwards.

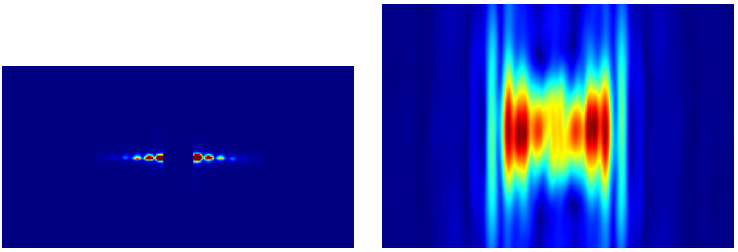

(a) Rotated average of diffraction.

(b) 2D projection of reconstructed microtubule.

Figure 6.4: Images showing the real rotated average diffraction and 2D projection of a reconstructed microtubule. 6.4a shows average of rotated diffraction patterns. 6.4b shows the reconstruction based on the averaged diffraction pattern.

The lack of higher-order diffraction peaks in figure 6.4a could be due to the nature of the data-processing. The way in which the liquid jet intentionally was kept unstable as well as exploded by the X-rays was likely to have changed the rotational orientation of the microtubules. Diffracting microtubules of a certain angle might then have higher-order diffraction at a different location than a diffracting microtubule of another angle. The rotation and averaging of these diffraction images might then dilute these higher-order effects, making them indifferentiable to noise. In order to investigate this a simple model of a microtubule was created and rotated in two planes with diffraction patterns for these models created for the different rotation angles. An example of one such simulation can be seen in figure 6.5.

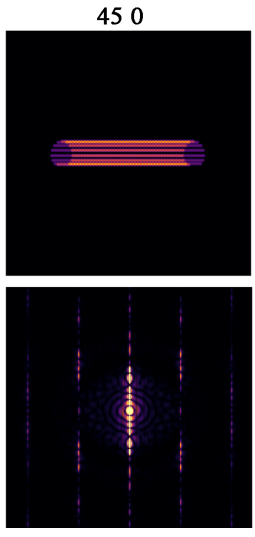

Figure 6.5: A simulation of diffraction from a simple model of microtubules. Top picture shows the microtubule and bottom picture shows corresponding diffraction pattern with higher order streaks. The numbers above indicate the rotation angles, in this case the microtubule is rotated 45° into the screen and 0° clockwise.

The different simulations for a variety of microtubule rotational angles were performed. The resulting diffraction patterns were radially integrated and plotted in order to determine if an averaging of differently rotated microtubules could diminish higher order effects. Curves resulting from radial integration of simulated data can be seen in figure 6.6.

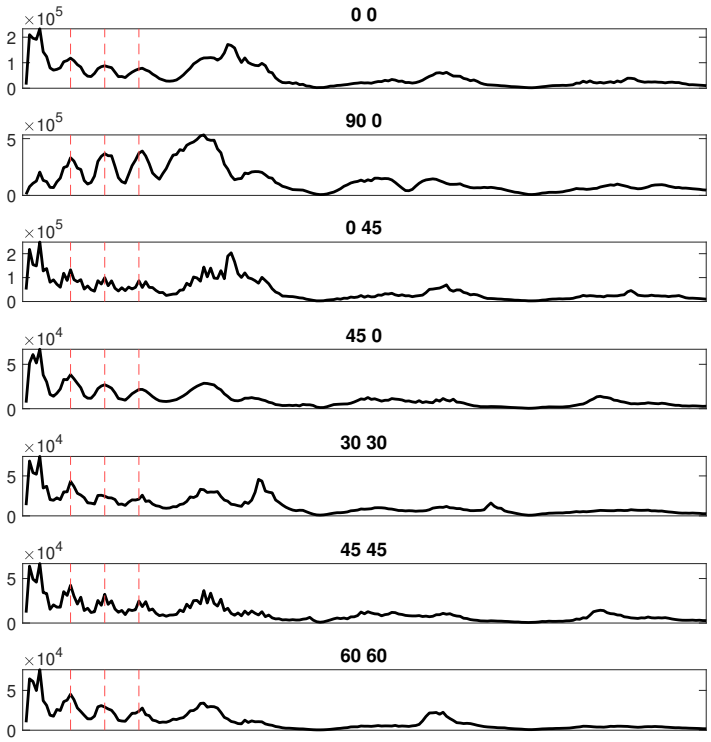

Figure 6.6: A number of radially integrated diffraction curves from simulated data. Numbers above each curve indicate rotation configuration of the microtubule. The x- and y-values are arbitrary and only serve to ease comparison between curves.

Results of the simulation in figure 6.6 indicate that the first few peaks in a radially integrated curve will appear in the same locations regardless of the orientation of the diffracting microtubule, only later peaks seem to differ significantly in location between differently angled microtubules. These later peaks should correspond to the higher-order diffraction peaks that are missing from figure 6.4a which makes it very likely that these higher-order effects are lost through averaging of images.

6.4 Final Comments and Conclusion

It is clear that more work needs to be done in order to properly analyse the data collected in this study. The unconventional approach to jetting used here circumvented the issue of jet diffraction overlapping microtubule diffraction, but at the price of complicating hit finding and analysis. A new hit finder could be designed that analyse intensities at higher diffraction angles in an attempt to differentiate between diffraction from microtubules oriented in different angles. Clustering algorithms could then be used to sort diffraction patterns into correlating groups, allowing for retrieval of a diffracting microtubule at its specific rotational angle.
A simulation package designed by Ariana Peck et al., called Skopi, allow for generation of diffraction images using models of a protein, such as a pdb-file [123]. Diffraction patterns can be made from single proteins at different angles, as well as numerous, or even clusters, of proteins. Using this simulation package it could be possible to use simulations of microtubule scattering in clusters or at different angles in order to aid in categorizing and identifying hits. If one could identify diffraction from microtubules at different angles and group these diffraction patterns it could potentially be possible to compare different diffraction groups, allowing for a more sophisticated reconstruction of the microtubule structure. Possibly even achieving a full 3D reconstruction of the microtubule. More work is definitely needed with the data obtained from this experiment.

Chapter 7

Concluding Remarks and Future Perspectives

In January of 2018 my PhD training started and I was quickly thrown into the crucible of preparing protein to be used in later experiments. The process of extracting tubulin from porcine brains as described in section 2.1 takes a full day of intense work. After a few initial days of protein extraction we had enough protein to last us through the experiments planned for the coming 6 months. During my five years of PhD-studies there would be many, many, more days of protein extraction.

One of the earlier things I was asked to do was to make some complementary measurements to an already completed study, or so we thought at the time. The study had used light scattering to look at polymerization of microtubules under the effects of electric fields in the GHz-range. The conclusion at the time was that these electric fields induced a non-thermal effect on microtubule polymerization. I was to perform a test using an IR-laser in order to make sure that thermophoresis (the transport of matter along a thermal gradient) had not influenced the result. I rebuilt the setup in order to conduct the complementary measurements and the resulting data showed that the IR-laser produced similar result as applying an electric field over the microtubules. After taking part in many more days of data collection, and a few weeks of rebuilding and improving the experimental setup, enough data was collected. I helped analyse the collected data and the conclusion was drawn that there was no non-thermal effect on the polymerization of microtubules as a result of exposure to GHz-fields. The thermal effects seen was not as a result of thermophoresis

either, but was chalked down to the effect of the thermal history of the sample. These findings are described in more detail in **paper 1**.

Another major aspect of my PhD-studies centered around the design of a device capable of delivering high-voltage electrical fields to a sample of polymerizing microtubules. The design of this device was done in cooperation with Electric Power Engineering at Chalmers University of Technology. Many hours went into designing and 3D-printing many different iterations until arriving at the design used in **paper 2**. After having designed the device I built the experimental setup, collected and analyzed the data, and took part in writing the manuscript. In the manuscript we conclude that only subtle effects of electromagnetic radiation with frequencies in the 100-240 kHz domain can be seen on polymerizing microtubules. These effects show a change in rate of polymerization in the second phase of the growth curve, most clearly for microtubules polymerizing under the effect of 147 kHz electric fields, which could be due to alignment of tubulin with the electric field.

The results presented in **paper 3** were obtained from an experiment that took place in the cSAXS beamline at the Swiss Light Source. Here we used TR-XSS to investigate the effects of microwave radiation on microtubules in solution. During the experiment I made myself as useful as I could: preparing protein sample, writing logbooks, and doing my part making sure that everything proceeded as smoothly as possible. After the experiment I was involved in the discourse regarding how to view and analyse the result. In the end the experiment showed that the only observable effects from microwaves on microtubules in solution were related to alignment, either with liquid flow or applied electric fields. These effects being so strong that if any vibrations within microtubules took place as a result of applied microwaves, they could not be seen. I took part in writing the manuscript where these conclusions were presented.

In **paper 4** we attempted to improve upon a previous paper made by the group [64]. We wanted to reconstruct the microtubule structure by collecting diffraction patterns taken from microtubules flowing in a liquid jet. During this project I helped apply and prepare for the beamtime at EuXFEL in Hamburg. I verified the experimental setup, both in house and at the beamline. I took part in data collection and later designed a hit finder to sift through the collected data. I analyzed much of the data

and took part in writing the manuscript. More work needs to be done on this project as we used an unconventional method during the data collection where we collected diffraction from an unstable jet. This was done in order to circumvent the issue of having diffraction from the liquid jet overlap with diffraction from microtubules. An unintended effect from this was that diffraction from differently angled microtubules aggravated the grouping of the resulting diffraction images. If diffraction patterns from differently angled microtubules can be properly grouped, a good reconstruction of the microtubule in a liquid environment is still possible.

With public concerns regarding high frequency fields and its potential effects on health still present [16–22] it is important to be careful when examining and presenting data related to this field of research. While the studies presented in this thesis show no strong non-thermal effects on microtubules polymerization or structure, it does not mean that they do not exist. The development of methods where one can reliably observe well organized, or even individual, microtubules under a variety of conditions could be very helpful when trying to determine the presence or absence of electric field induced effects on said proteins. Examples of existing techniques that could be explored as a basis to achieve this could be electrospraying, where imaging of single biomolecules in liquid has been achieved, or microfluidic channels, that has shown the possibility of polymerizing microtubules unidirectionally [124, 125]. The choice of approach going forward will result in issues unique for that particular technique. Finding a balance between producing solutions or workarounds for each issue, and realising when one should try a whole new approach will, as in so many things, be key.

This thesis has been an attempt at summarizing the five year journey towards my PhD. As with many summaries it is difficult to provide a concise text that explains everything without losing information along the way. Instead one tries to describe the essence of the thoughts and decisions that led one to conduct the work that in the end is presented with tentative pride. Tentative, because one can never turn every single stone and look at a problem from every single perspective, and some small aspect will inevitably be overlooked. There is, after all, nothing like hindsight to make one realize that some stones should have been turned much earlier, while

other stones need not have been turned at all. However, with no end of stones in sight, all you can do is keep turning them.

Bibliography

[1] R. Schmitt, *Electromagnetics Explained: A Handbook for Wireless/RF, EMC, and High-Speed Electronics*. Newnes, 05 2002.

[2] D. M. Cook, *The theory of the electromagnetic field*. Dover Publications, 2002.

[3] H. Fröhlich, "Long-range coherence and energy storage in biological systems," *International Journal of Quantum Chemistry*, vol. 2, pp. 641–649, 9 1968.

[4] H. Frohlich, "The extraordinary dielectric properties of biological materials and the action of enzymes," *Proceedings of the National Academy of Sciences of the United States of America*, vol. 72, pp. 4211–4215, 1975.

[5] A. S. Dawe, B. Smith, D. W. P. Thomas, S. Greedy, N. Vasic, A. Gregory, B. Loader, and D. I. D. Pomerai, "A small temperature rise may contribute towards the apparent induction by microwaves of heat-shock gene expression in the nematode caenorhabditis elegans," *Bioelectromagnetics*, vol. 27, pp. 88–97, 2006.

[6] D. D. Pomerai, C. Daniells, H. David, J. Allan, I. Duce, M. Mutwakil, D. Thomas, P. Sewell, J. Tattersall, D. Jones, and P. Candido, "Non-thermal heat-shock response to microwaves," *Nature 2000 405:6785*, vol. 405, pp. 417–418, 5 2000.

[7] D. I. D. Pomerai, B. Smith, A. Dawe, K. North, T. Smith, D. B. Archer, I. R. Duce, D. Jones, and E. P. M. Candido, "Microwave radiation can alter protein conformation without bulk heating," *FEBS Letters*, vol. 543, pp. 93–97, 5 2003.

[8] J. H. Lim, S. D. McCullen, J. A. Piedrahita, E. G. Loboa, and N. J. Olby, "Alternating current electric fields of varying frequencies: Effects on proliferation and differentiation of porcine neural progenitor cells," *Cellular Reprogramming*, vol. 15, p. 405, 10 2013.

[9] A. Sinelnikova, T. Mandl, H. Agelii, O. Gråsäs, E. G. Marklund, C. Caleman, and E. D. Santis, "Protein orientation in time-dependent electric fields: orientation before destruction," *Biophysical Journal*, vol. 120, pp. 3709–3717, 9 2021.

[10] Q. Zhang, D. Shao, P. Xu, and Z. Jiang, "Effects of an electric field on the conformational transition of the protein: Pulsed and oscillating electric fields with different frequencies," *Polymers*, vol. 14, 1 2021.

[11] X. Tao, A. Lee, W. Limapichat, D. A. Dougherty, and R. MacKinnon, "A gating charge transfer center in voltage sensors," *Science (New York, N.Y.)*, vol. 328, p. 67, 4 2010.

[12] Y. Murata, H. Iwasaki, M. Sasaki, K. Inaba, and Y. Okamura, "Phosphoinositide phosphatase activity coupled to an intrinsic voltage sensor," *Nature*, vol. 435, pp. 1239–1243, 6 2005.

[13] C. M. Armstrong and F. Bezanilla, "Charge movement associated with the opening and closing of the activation gates of the na channels," *The Journal of General Physiology*, vol. 63, p. 533, 5 1974.

[14] S. A. Seoh, D. Sigg, D. M. Papazian, and F. Bezanilla, "Voltage-sensing residues in the s2 and s4 segments of the shaker k+ channel," *Neuron*, vol. 16, pp. 1159–1167, 1996.

[15] D. R. Hekstra, K. I. White, M. A. Socolich, R. W. Henning, V. Šrajer, and R. Ranganathan, "Electric-field-stimulated protein mechanics," *Nature Publishing Group*, 2016.

[16] K. Karipidis, R. Mate, D. Urban, R. Tinker, and A. Wood, "5g mobile networks and health—a state-of-the-science review of the research into low-level rf fields above 6 ghz," *Journal of Exposure Science & Environmental Epidemiology 2021 31:4*, vol. 31, pp. 585–605, 3 2021.

[17] I. A. Cotgreave, "Biological stress responses to radio frequency electromagnetic radiation: are mobile phones really so (heat) shocking?," *Archives of biochemistry and biophysics*, vol. 435, pp. 227–240, 3 2005.

[18] I. Belyaev, "Nonthermal biological effects of microwaves: Current knowledge, further perspective, and urgent needs," *Electromagnetic Biology and Medicine*, vol. 24, pp. 375–403, 2005.

[19] D. J. Panagopoulos, O. Johansson, and G. L. Carlo, "Polarization: A key difference between man-made and natural electromagnetic fields, in regard to biological activity," *Scientific Reports 2015 5:1*, vol. 5, pp. 1–10, 10 2015.

[20] J. Skinner, T. J. Mee, R. P. Blackwell, M. P. Maslanyj, J. Simpson, S. G. Allen, and N. E. Day, "Exposure to power frequency electric fields and the risk of childhood cancer in the uk," *British Journal of Cancer 2002 87:11*, vol. 87, pp. 1257–1266, 11 2002.

[21] F. D. Vocht, ""dirty electricity": what, where, and should we care?," *Journal of Exposure Science & Environmental Epidemiology 2010 20:5*, vol. 20, pp. 399–405, 3 2010.

[22] A. Ramundo-Orlando, "Effects of millimeter waves radiation on cell membrane - a brief review," *Journal of Infrared, Millimeter, and Terahertz Waves*, vol. 31, pp. 1400–1411, 12 2010.

[23] G. Ziegelberger, R. Croft, M. Feychting, A. C. Green, A. Hirata, G. d'Inzeo, K. Jokela, S. Loughran, C. Marino, S. Miller, G. Oftedal, T. Okuno, E. van Rongen, M. Röösli, Z. Sienkiewicz, J. Tattersall, and S. Watanabe, "Guidelines for limiting exposure to electromagnetic fields (100 khz to 300 ghz)," *Health Physics*, vol. 118, pp. 483–524, 5 2020.

[24] M. Ohring and L. Kasprzak, "Electronic devices: How they operate and are fabricated," *Reliability and Failure of Electronic Materials and Devices*, pp. 39–109, 1 2015.

[25] E. D. Kirson, Z. Gurvich, R. Schneiderman, E. Dekel, A. Itzhaki, Y. Wasserman, R. Schatzberger, and Y. Palti, "Disruption of cancer cell replication by alternating electric fields," *Cancer Research*, vol. 64, pp. 3288–3295, 2004.

[26] E. D. Kirson, V. Dbalý, F. Tovaryš, J. Vymazal, J. F. Soustiel, A. Itzhaki, D. Mordechovich, S. Steinberg-Shapira, Z. Gurvich, R. Schneiderman, Y. Wasserman, M. Salzberg, B. Ryffel, D. Goldsher, E. Dekel, and Y. Palti, "Alternating electric fields arrest cell proliferation in animal tumor models and human brain tumors," *Proceedings of the National Academy of Sciences of the United States of America*, vol. 104, p. 10152, 6 2007.

[27] J. A. Tuszynski, C. Wenger, D. E. Friesen, and J. Preto, "An overview of sub-cellular mechanisms involved in the action of ttfields," *International Journal of Environmental Research and Public Health*, vol. 13, 11 2016.

[28] K. W. Carlson, J. A. Tuszynski, S. Dokos, N. Paudel, T. Dreeben, and Z. Bomzon, "How do tumor-treating fields work?," *Brain and Human Body Modeling 2020*, pp. 19–35, 2021.

[29] A. G. V. D. Heijden, L. A. Kiemeney, O. N. Gofrit, O. Nativ, A. Sidi, Z. Leib, R. Colombo, R. Naspro, M. Pavone, J. Baniel, F. Hasner, and J. A. Witjes, "Preliminary european results of local microwave hyperthermia and chemotherapy treatment in intermediate or high risk superficial transitional cell carcinoma of the bladder," *European Urology*, vol. 46, pp. 65–72, 7 2004.

[30] N. R. Datta, A. K. Bose, H. K. Kapoor, and S. Gupta, "International journal of hyperthermia head and neck cancers: Results of thermoradiotherapy versus radiotherapy head and neck cancers: results of thermoradiotherapy versus radiotherapy," *Int. J. Hyperthermxa*, vol. 6, pp. 479–486, 1990.

[31] G. M. Cooper., *The Cell: A Molecular Approach.* Sunderland (MA), 2nd ed., 2000.

[32] A. P. Kalra, B. B. Eakins, S. D. Patel, G. Ciniero, V. Rezania, K. Shankar, and J. A. Tuszynski, "All wired up: An exploration of the electrical properties of microtubules and tubulin," *ACS Nano*, vol. 14, pp. 16301–16320, 12 2020.

[33] A. Kalra, S. Patel, A. Bhuiyan, J. Preto, K. Scheuer, U. Mohammed, J. Lewis, V. Rezania, K. Shankar, and J. A. Tuszynski, "On the capacitive properties of individual microtubules and their meshworks," *Scientific Reports 2020 10:1*, vol. 10, pp. 1–11, 5 2019.

[34] M. G. V. D. Heuvel, M. P. D. Graaff, and C. Dekker, "Molecular sorting by electrical steering of microtubules in kinesin-coated channels," *Science*, vol. 312, pp. 910–914, 5 2006.

[35] M. Giladi, R. S. Schneiderman, T. Voloshin, Y. Porat, M. Munster, R. Blat, S. Sherbo, Z. Bomzon, N. Urman, A. Itzhaki, S. Cahal, A. Shteingauz, A. Chaudhry, E. D. Kirson, U. Weinberg, and Y. Palti, "Mitotic spindle disruption by alternating electric fields leads to improper chromosome segregation and mitotic catastrophe in cancer cells.," *Scientific Reports*, vol. 5, pp. 18046–18046, 12 2015.

[36] J. J. Timmons, J. Preto, J. A. Tuszynski, and E. T. Wong, "Tubulin's response to external electric fields by molecular dynamics simulations," *PLoS ONE*, vol. 13, 9 2018.

[37] B. Alberts, D. Bray, K. Hopkins, A. Johnson, J. Lewis, M. Raff, K. Roberts, and P. Walter, "Essential cell biology fourth edition," *Garland Science*, p. 728, 2014.

[38] S. Wilkinson and A. Marcus, "Cytoskeletal proteins," 2016.

[39] E. Krauhs, M. Little, T. Kempf, R. Hofer-Warbinek, W. Ade, and H. Ponstingl, "Complete amino acid sequence of β-tubulin from porcine brain," *Proceedings of the National Academy of Sciences of the United States of America*, vol. 78, pp. 4156–4160, 1981.

[40] R. H. Wade, D. Chrétien, and D. Job, "Characterization of microtubule protofilament numbers: How does the surface lattice accommodate?," *Journal of Molecular Biology*, vol. 212, pp. 775–786, 4 1990.

[41] S. Chaaban and G. J. Brouhard, "A microtubule bestiary: structural diversity in tubulin polymers," *Molecular Biology of the Cell*, vol. 28, p. 2924, 11 2017.

[42] E. T. Nsamba, A. Bera, M. Costanzo, C. Boone, and M. L. G. Jr., "Tubulin isotypes optimize distinct spindle positioning mechanisms during yeast mitosis," *Journal of Cell Biology*, vol. 220, p. e202010155, 11 2021.

[43] E. T. Nsamba and M. L. G. Jr, "Tubulin isotypes – functional insights from model organisms," *Journal of Cell Science*, vol. 135, p. jcs259539, 5 2022.

[44] F. Montecinos-Franjola, S. K. Chaturvedi, P. Schuck, and D. L. Sackett, "All tubulins are not alike: Heterodimer dissociation differs among different biological sources," *Journal of Biological Chemistry*, vol. 294, pp. 10315–10324, 6 2019.

[45] T. Mitchison and M. Kirschner, "Dynamic instability of microtubule growth," *Nature 1984 312:5991*, vol. 312, pp. 237–242, 1984.

[46] A. Akhmanova and M. O. Steinmetz, "Tracking the ends: a dynamic protein network controls the fate of microtubule tips," *Nature Reviews Molecular Cell Biology 2008 9:4*, vol. 9, pp. 309–322, 4 2008.

[47] M. F. Carlier and D. Pantaloni, "Kinetic analysis of guanosine 5'-triphosphate hydrolysis associated with tubulin polymerization," *Biochemistry*, vol. 20, pp. 1918–1924, 1981.

[48] A. Desai and T. J. Mitchison, "Microtubule polymerization dynamics," *Annual review of cell and developmental biology*, vol. 13, pp. 83–117, 1997.

[49] D. Kuchnir Fygenson, H. Flyvbjerg, K. Sneppen, A. Libchaber, and S. Leibler, "Spontaneous nucleation of microtubules," *Phys. Rev. E*, vol. 51, pp. 5058–5063, May 1995.

[50] R. Audenaert, L. Heremans, K. Heremans, and Y. Engelborghs, "Secondary structure analysis of tubulin and microtubules with raman spectroscopy," *Biochimica et Biophysica Acta (BBA) - Protein Structure and Molecular Enzymology*, vol. 996, pp. 110–115, 6 1989.

[51] H. T. Schek, M. K. Gardner, J. Cheng, D. J. Odde, and A. J. Hunt, "Microtubule assembly dynamics at the nanoscale," *Current biology : CB*, vol. 17, p. 1445, 9 2007.

[52] J. Howard and A. A. Hyman, "Dynamics and mechanics of the microtubule plus end," *Nature*, vol. 422, pp. 753–758, 2003.

[53] C. M. Galmarini, K. Kamath, A. Vanier-Viornery, V. Hervieu, E. Peiller, N. Falette, A. Puisieux, M. A. Jordan, and C. Dumontet, "Drug resistance associated with loss of p53 involves extensive alterations in microtubule composition and dynamics," *British Journal of Cancer*, vol. 88, p. 1793, 6 2003.

[54] P. Fortugno, N. R. Wall, A. Giodini, D. S. O'Connor, J. Plescia, K. M. Padgett, S. Tognin, P. C. Marchisio, and D. C. Altieri, "Survivin exists in immunochemically distinct subcellular pools and is involved in spindle microtubule function," *Journal of Cell Science*, vol. 115, pp. 575–585, 2 2002.

[55] M. A. Jordan and L. Wilson, "Microtubules and actin filaments: dynamic targets for cancer chemotherapy," *Current opinion in cell biology*, vol. 10, pp. 123–130, 1998.

[56] L. Wilson, D. Panda, and M. A. Jordan, "Modulation of microtubule dynamics by drugs: a paradigm for the actions of cellular regulators," *Cell structure and function*, vol. 24, pp. 329–335, 1999.

[57] N. H. Oberlies and D. J. Kroll, "Camptothecin and taxol: Historic achievements in natural products research," *Journal of Natural Products*, vol. 67, pp. 129–135, 2 2004.

[58] F. A. Holmes, R. S. Walters, R. L. Theriault, A. U. Buzdar, D. K. Frye, G. N. Hortobagyi, A. D. Forman, L. K. Newton, and M. N. Raber, "Phase ii trial of taxol, an active drug in the treatment of metastatic breast cancer," *Journal of the National Cancer Institute*, vol. 83, pp. 1797–1805, 12 1991.

[59] S. Kumar, H. Mahdi, C. Bryant, J. P. Shah, G. Garg, and A. Munkarah, "Clinical trials and progress with paclitaxel in ovarian cancer," *International Journal of Women's Health*, vol. 2, p. 411, 2010.

[60] P. A. Francis, M. G. Kris, J. R. Rigas, S. C. Grant, and V. A. Miller, "Paclitaxel (taxol) and docetaxel (taxotere): active chemotherapeutic agents in lung cancer," *Lung Cancer*, vol. 12, 1995.

[61] P. B. Schiff, J. Fant, and S. B. Horwitz, "Promotion of microtubule assembly in vitro by taxol," *Nature*, vol. 277, pp. 665–667, 1979.

[62] I. Arnal and R. H. Wade, "How does taxol stabilize microtubules?," *Current Biology*, vol. 5, pp. 900–908, 1995.

[63] L. A. Amos and J. Löwe, "How taxol® stabilises microtubule structure," *Chemistry & Biology*, vol. 6, pp. R65–R69, 3 1999.

[64] G. Brändén, G. Hammarin, R. Harimoorthy, A. Johansson, D. Arnlund, E. Malmerberg, A. Barty, S. Tångefjord, P. Berntsen, D. P. DePonte, C. Seuring, T. A. White, F. Stellato, R. Bean, K. R. Beyerlein, L. M. Chavas, H. Fleckenstein, C. Gati, U. Ghoshdastider, L. Gumprecht, D. Oberthür, D. Popp, M. Seibert, T. Tilp, M. Messerschmidt, G. J. Williams, N. D. Loh, H. N. Chapman, P. Zwart, M. Liang, S. Boutet, R. C. Robinson, and R. Neutze, "Coherent diffractive imaging of microtubules using an x-ray laser," *Nature Communications 2019 10:1*, vol. 10, pp. 1–9, 6 2019.

[65] P. Meurer-Grob, J. Kasparian, and R. H. Wade, "Microtubule structure at improved resolution," *Biochemistry*, vol. 40, pp. 8000–8008, 7 2001.

[66] E. Nogales, S. G. Wolf, and K. H. Downing, "Structure of the tubulin dimer by electron crystallography," *Nature*, vol. 391, 1998.

[67] R. R. Ramalho, H. Soares, and L. V. Melo, "Microtubule behavior under strong electromagnetic fields," *Materials Science and Engineering C*, vol. 27, pp. 1207–1210, 2007.

[68] M. G. V. D. Heuvel, M. P. D. Graaff, S. G. Lemay, and C. Dekker, "Electrophoresis of individual microtubules in microchannels," *Proceedings of the National Academy of Sciences of the United States of America*, vol. 104, pp. 7770–7775, 5 2007.

[69] S. R. Hameroff and R. C. Watt, "Information processing in microtubules," *Journal of Theoretical Biology*, vol. 98, pp. 549–561, 10 1982.

[70] S. Hameroff and R. Penrose, "Consciousness in the universe: A review of the 'orch or' theory," *Physics of Life Reviews*, vol. 11, pp. 39–78, 3 2014.

[71] T. J. A. Craddock, S. R. Hameroff, A. T. Ayoub, M. Klobukowski, and J. A. Tuszynski, "Anesthetics act in quantum channels in brain microtubules to prevent consciousness," *Current Topics in Medicinal Chemistry*, vol. 15, pp. 523–533, 2 2015.

[72] J. Pokorný, F. Jelínek, and V. Trkal, "Electric field around microtubules," *Bioelectrochemistry and Bioenergetics*, vol. 45, pp. 239–245, 5 1998.

[73] K. R. Foster and J. W. Baish, "Viscous damping of vibrations in microtubules," *Journal of Biological Physics*, vol. 26, pp. 255–260, 2000.

[74] J. Pokorný, "Viscous effects on polar vibrations in microtubules," *Electromagnetic Biology and Medicine*, vol. 22, pp. 15–29, 2003.

[75] J. Jacob, L. H. L. Chia, and F. Y. C. Boey, "Review thermal and non-thermal interaction of microwave radiation with materials," *Journal of Materials Science*, vol. 30, pp. 5321–5327, 1995.

[76] A. Andryieuski, S. M. Kuznetsova, S. V. Zhukovsky, Y. S. Kivshar, and A. V. Lavrinenko, "Water: Promising opportunities for tunable all-dielectric electromagnetic metamaterials," *Scientific Reports*, vol. 5, 8 2015.

[77] S. Jiang and S. Georgakopoulos, "Electromagnetic wave propagation into fresh water," *Journal of Electromagnetic Analysis and Applications*, vol. 3, pp. 261–266, 2011.

[78] G. Butcher, J. Mottar, C. L. Parkinson, and E. J. Wollack, *Tour of the electromagnetic spectrum*. National Aeronautics and Space Administration, 3 ed., 2016.

[79] G. S. Smith, *An Introduction To Classical Electromagnetic Radiation*. Cambridge University Press, 8 1997.

[80] "The electromagnetic spectrum - mini physics - learn physics." available at `https://www.miniphysics.com/electromagnetic-spectrum_25.html`.

[81] E. N. D. C. Andrade, "Christian huygens and the development of science in the seventeenth century," *Nature 1948 162:4117*, vol. 162, pp. 472–473, 9 1948.

[82] J. Peatross and M. Ware, *Physics of Light and Optics: A Free Online Textbook*. Optica Publishing Group, 10 2010.

[83] H. G. Kraus, "Huygens–fresnel–kirchhoff wave-front diffraction formulation: spherical waves," *JOSA A, Vol. 6, Issue 8, pp. 1196-1205*, vol. 6, pp. 1196–1205, 8 1989.

[84] M. Mansuripur, "A tutorial on the classical theories of electromagnetic scattering and diffraction," *Nanophotonics*, vol. 10, pp. 315–342, 9 2020.

[85] "diffraction | definition, examples, types, & facts - britannica." `https://www.britannica.com/science/diffraction`.

[86] M. J. Berg and C. M. Sorensen, "A review and reassessment of diffraction, scattering, and shadows in electrodynamics," *Journal of Quantitative Spectroscopy & Radiative Transfer*, vol. 210, pp. 225–239, 2018.

[87] S. Chakraborty, R. Venkatramani, B. J. Rao, B. Asgeirsson, and A. M. Dandekar, "Protein structure quality assessment based on the distance profiles of consecutive backbone cα atoms," *F1000Research*, vol. 2, 12 2013.

[88] V. I. Mikla, V. I. Rusin, and P. A. Boldizhar, "Advances in imaging from the first x-ray images," *Journal of Optoelectronics and Advanced Materials*, vol. 14, pp. 559–570, 2012.

[89] N. Huang, H. Deng, B. Liu, D. Wang, and Z. Zhao, "Features and futures of x-ray free-electron lasers," *The Innovation*, vol. 2, p. 100097, 5 2021.

[90] C. Pellegrini, "The development of xfels," *Nature Reviews Physics*, vol. 2, pp. 330–331, 2020.

[91] C. Pellegrini and J. Stöhr, "X-ray free-electron lasers—principles, properties and applications," *Nuclear Instruments and Methods in Physics Research Section A: Accelerators, Spectrometers, Detectors and Associated Equipment*, vol. 500, pp. 33–40, 3 2003.

[92] P. S. Rahimabadi, M. Khodaei, and K. R. Koswattage, "Review on applications of synchrotron-based x-ray techniques in materials characterization," *X-Ray Spectrometry*, vol. 49, pp. 348–373, 5 2020.

[93] P. Willmott, "An introduction to synchrotron radiation," *An Introduction to Synchrotron Radiation*, 3 2019.

[94] P. R. Willmott, "X-ray sources at large-scale facilities," *Springer Proceedings in Physics*, vol. 262, pp. 1–37, 2021.

[95] O. Glatter and O. Kratky, *Small Angle X-Ray Scattering*. 24/28 Oval Road, London: Academic Press Inc, 1982.

[96] M. A. Graewert and D. I. Svergun, "Impact and progress in small and wide angle x-ray scattering (saxs and waxs)," *Current Opinion in Structural Biology*, vol. 23, pp. 748–754, 10 2013.

[97] A. G. Kikhney and D. I. Svergun, "A practical guide to small angle x-ray scattering (saxs) of flexible and intrinsically disordered proteins," *FEBS Letters*, vol. 589, pp. 2570–2577, 9 2015.

[98] M. Castoldi and A. V. Popov, "Purification of brain tubulin through two cycles of polymerization–depolymerization in a high-molarity buffer," *Protein Expression and Purification*, vol. 32, pp. 83–88, 11 2003.

[99] J. Roostalu and T. Surrey, "Microtubule nucleation: beyond the template," *Nature Reviews Molecular Cell Biology 2017 18:11*, vol. 18, pp. 702–710, 8 2017.

[100] D. Job, O. Valiron, and B. Oakley, "Microtubule nucleation," *Current Opinion in Cell Biology*, vol. 15, pp. 111–117, 2 2003.

[101] W. A. Voter and H. P. Erickson, "The kinetics of microtubule assembly. evidence for a two-stage nucleation mechanism.," *Journal of Biological Chemistry*, vol. 259, pp. 10430–10438, 8 1984.

[102] K. A. Johnson and G. G. Borisy, "Kinetic analysis of microtubule self-assembly in vitro," *Journal of Molecular Biology*, vol. 117, pp. 1–31, 11 1977.

[103] D. I. Stimpson and V. A. Bloomfield, "Physical properties of rod-shaped molecules in solution," *Biopolymers*, vol. 24, pp. 387–402, 1985.

[104] B. E. Warren, *X-ray Diffraction*. Dover puplications, 1990.

[105] L. A. Feigin and D. I. Svergun, *Structure Analysis by Small-Angle X-Ray and Neutron Scattering*. Plenum Publishing Corporation, 1987.

[106] D. K. Putnam, E. W. Lowe, and J. Meiler, "Reconstruction of saxs profiles from protein structures," *Computational and Structural Biotechnology Journal*, vol. 8, p. e201308006, 2013.

[107] J. Miao, P. Charalambous, J. Kirz, and D. Sayre, "Extending the methodology of x-ray crystallography to allow imaging of micrometre-sized non-crystalline specimens," *Nature*, vol. 400, pp. 342–344, 1999.

[108] R. Henderson, "The potential and limitations of neutrons, electrons and x-rays for atomic resolution microscopy of unstained biological molecules," *Quarterly Reviews of Biophysics*, vol. 28, pp. 171–193, 1995.

[109] R. Henderson, "Cryo-protection of protein crystals against radiation damage in electron and x-ray diffraction," *Proceedings of the Royal Society of London. Series B: Biological Sciences*, vol. 241, pp. 6–8, 7 1990.

[110] R. Neutze, R. Wouts, D. van der Spoel, E. Weckert, and J. Hajdu, "Potential for biomolecular imaging with femtosecond x-ray pulses," *Nature*, vol. 406, pp. 752–757, 2000.

[111] A. V. Martin, F. Wang, N. D. Loh, T. Ekeberg, F. R. N. C. Maia, M. Hantke, G. van der Schot, C. Y. Hampton, R. G. Sierra, A. Aquila, S. Bajt, M. Barthelmess, C. Bostedt, J. D. Bozek, N. Coppola, S. W. Epp, B. Erk, H. Fleckenstein, L. Foucar, M. Frank, H. Graafsma, L. Gumprecht, A. Hartmann, R. Hartmann, G. Hauser, H. Hirsemann, P. Holl, S. Kassemeyer, N. Kimmel, M. Liang, L. Lomb, S. Marchesini, K. Nass, E. Pedersoli, C. Reich, D. Rolles, B. Rudek, A. Rudenko, J. Schulz, R. L. Shoeman, H. Soltau, D. Starodub, J. Steinbrener, F. Stellato, L. StrüderStr, J. Ullrich, G. Weidenspointner, T. A. White, C. B. Wunderer, A. Barty, I. Schlichting, M. J. Bogan, H. N. Chapman, A. Noy, S. P. Hau-Riege, C. Cui, M. R. Howells, R. Rosen, H. He, J. C. H. Spence, U. Weierstall, T. Beetz, C. Jacobsen, S. Boutet, B. W. Woods, W. H. Benner, R. A. London, E. Plönjes, M. Kuhlmann, R. Treusch, S. Düsterer, T. Tschentscher, J. R. Schneider, E. Spiller, T. Möller, M. Hoener, D. A. Shapiro, K. O. Hodgson, D. van der Spoel, F. Burmeister, M. Bergh, C. Caleman, G. Huldt, M. M. Seibert, R. W. Lee, A. Szöke, N. Tim-neanu, J. Hajdu, W. J. Huang, R. Sun, J. Tao, L. D. Menard, R. G. Nuzzo, and J. M. Zuo, "Noise-robust coherent diffractive imaging with a single diffraction pattern," *Optics Express, Vol. 20, Issue 15, pp. 16650-16661*, vol. 20, pp. 16650–16661, 7 2012.

[112] M. Cammarata, M. Levantino, F. Schotte, P. A. Anfinrud, F. Ewald, J. Choi, A. Cupane, M. Wulff, and H. Ihee, "Tracking the structural dynamics of proteins in solution using time-resolved wide-angle x-ray scattering," *Nature Methods*, vol. 5, pp. 881–886, 2008.

[113] M. Andersson, E. Malmerberg, S. Westenhoff, G. Katona, M. Cammarata, A. B. Wöhri, L. C. Johansson, F. Ewald, M. Eklund, M. Wulff, J. Davidsson, and R. Neutze, "Structural dynamics of light-driven proton pumps," *Structure*, vol. 17, pp. 1265–1275, 9 2009.

[114] E. Malmerberg, P. H. Bovee-Geurts, G. Katona, X. Deupi, D. Arnlund, C. Wickstrand, L. C. Johansson, S. Westenhoff, E. Nazarenko, G. F. Schertler, A. Menzel, W. J. D. Grip, and R. Neutze, "Conformational activation of visual rhodopsin in native disc membranes," *Science Signaling*, vol. 8, 3 2015.

[115] M. Levantino, G. Schirò, H. T. Lemke, G. Cottone, J. M. Glownia, D. Zhu, M. Chollet, H. Ihee, A. Cupane, and M. Cammarata, "Ultrafast myoglobin structural dynamics observed with an x-ray free-electron laser," *Nature Communications 2015 6:1*, vol. 6, pp. 1–6, 4 2015.

[116] H. S. Choa, N. Dashdorj, F. Schotte, T. Graber, R. Henning, and P. Anfinrud, "Protein structural dynamics in solution unveiled via 100-ps time-resolved x-ray scattering," *Proceedings of the National Academy of Sciences of the United States of America*, vol. 107, pp. 7281–7286, 4 2010.

[117] D. Arnlund, L. C. Johansson, C. Wickstrand, A. Barty, G. J. Williams, E. Malmerberg, J. Davidsson, D. Milathianaki, D. P. DePonte, R. L. Shoeman, D. Wang, D. James, G. Katona, S. Westenhoff, T. A. White, A. Aquila, S. Bari, P. Berntsen, M. Bogan, T. B. V. Driel, R. B. Doak, K. S. Kjær, M. Frank, R. Fromme, I. Grotjohann, R. Henning, M. S. Hunter, R. A. Kirian, I. Kosheleva, C. Kupitz, M. Liang, A. V. Martin, M. M. Nielsen, M. Messerschmidt, M. M. Seibert, J. Sjöhamn, F. Stellato, U. Weierstall, N. A. Zatsepin, J. C. Spence, P. Fromme, I. Schlichting, S. Boutet, G. Groenhof, H. N. Chapman, and R. Neutze, "Visualizing a protein quake with time-resolved x-ray scattering at a free-electron laser," *Nature Methods 2014 11:9*, vol. 11, pp. 923–926, 8 2014.

[118] D. Sarabi, L. Ostojić, R. Bosman, A. Vallejos, J.-B. Linse, M. Wulff, M. Levantino, and R. Neutze, "Modeling difference x-ray scattering observations from an integral membrane protein within a detergent micelle," *Structural Dynamics*, vol. 9, p. 054102, 10 2022.

[119] R. Harimoorthy, "Effect of microwaves on microtubule structure and function probed by light and x-ray scattering," 4 2018.

[120] K. J. Böhm, N. E. Mavromatos, A. Michette, R. Stracke, and E. Unger, "Movement and alignment of microtubules in electric fields and electric-dipole-moment estimates," *Electromagnetic Biology and Medicine*, vol. 24, pp. 319–330, 2005.

[121] M. A. Schroer, S. Schewa, A. Y. Gruzinov, C. Rönnau, J. M. Lahey-Rudolph, C. E. Blanchet, T. Zickmantel, Y. H. Song, D. I. Svergun, and M. Roessle, "Probing the existence of non-thermal terahertz radiation induced changes of the protein solution structure," *Scientific Reports 2021 11:1*, vol. 11, pp. 1–13, 11 2021.

[122] M. M. Seibert, S. Boutet, M. Svenda, al, J. Fu, P. Li, D. P. DePonte, U. Weierstall, K. Schmidt, J. Warner, D. Starodub, J. C. H. Spence, and R. B. Doak, "Gas dynamic virtual nozzle for generation of microscopic droplet streams," *Journal of Physics D: Applied Physics*, vol. 41, p. 195505, 9 2008.

[123] A. Peck, H.-Y. Chang, A. Dujardin, D. Ramalingam, M. Uervirojnangkoorn, Z. Wang, A. Mancuso, F. Poitevin, and C. H. Yoon, "Skopi: a simulation package for diffractive imaging of noncrystalline biomolecules," *Journal of Applied Crystallography*, vol. 55, pp. 1002–1010, 8 2022.

[124] J. Bielecki, M. F. Hantke, B. J. Daurer, H. K. N. Reddy, D. Hasse, D. S. D. Larsson, L. H. Gunn, M. Svenda, A. Munke, J. A. Sellberg, L. Flueckiger, A. Pietrini, C. Nettelblad, I. Lundholm, G. Carlsson, K. Okamoto, N. Timneanu, D. Westphal, O. Kulyk, A. Higashiura, G. van der Schot, N.-T. D. Loh, T. E. Wysong, C. Bostedt, T. Gorkhover, B. Iwan, M. M. Seibert, T. Osipov, P. Walter, P. Hart, M. Bucher, A. Ulmer, D. Ray, G. Carini, K. R. Ferguson, I. Andersson, J. Andreasson, J. Hajdu, and F. R. N. C. Maia, "Electrospray sample injection for single-particle imaging with x-ray lasers," *Science Advances*, vol. 5, p. eaav8801, 2019.

[125] J. H. Liu, K. C. Hsia, R. Yokokawa, and Y. W. Lu, "Microtubule polymerization in alignment by an on-chip temperature gradient platform," *Sensors and Actuators B: Chemical*, vol. 298, p. 126813, 11 2019.